THERMAL STRESS INTENSITY FACTOR EVALUATION FOR INCLINED CRACKS IN FUNCTIONALLY GRADED MATERIALS USING J_k -INTEGRAL METHOD

A THESIS SUBMITTED TO
THE GRADUATE SCHOOL OF NATURAL AND APPLIED SCIENCES
OF
MIDDLE EAST TECHNICAL UNIVERSITY

BY

BENGİ DEMİRÇİVİ

IN PARTIAL FULFILLMENT OF THE REQUIREMENTS
FOR
THE DEGREE OF MASTER OF SCIENCE
IN
MECHANICAL ENGINEERING

NOVEMBER 2006

Approval of the Graduate School of Natural and Applied Sciences

_____

Prof. Dr. Canan ÖZGEN
Director

I certify that this thesis satisfies all the requirements as a thesis for the degree of Master of Science.

_____

Prof. Dr. S. Kemal İDER
Head of Department

This is to certify that we have read this thesis and that in our opinion it is fully adequate, in scope and quality, as a thesis for the degree of Master of Science.

_____

Asst. Prof. Dr. Serkan DAĞ
Supervisor

Examining Committee Members

Head of Jury : Prof. Dr. Metin AKKÖK (METU, ME) _____

Supervisor: Asst. Prof. Dr. Serkan DAĞ (METU, ME) _____

Prof. Dr. Bülent DOYUM (METU, ME) _____

Assoc. Prof. Dr. Suat KADIOĞLU (METU, ME) _____

Assoc. Prof. Dr. Bora YILDIRIM (Hacettepe Univ, ME) _____

I hereby declare that all information in this document has been obtained and presented in accordance with academic rules and ethical conduct. I also declare that, as required by these rules and conduct, I have fully cited and referenced all material and results that are not original to this work.

Name, Lastname : Bengi DEMİRÇİVİ

Signature :

ABSTRACT

THERMAL STRESS INTENSITY FACTOR EVALUATION
FOR
INCLINED CRACKS IN FUNCTIONALLY GRADED MATERIALS
USING J_k-INTEGRAL METHOD

Demirçivi, Bengi

M.S., Department of Mechanical Engineering

Supervisor: Asst. Prof. Dr. Serkan DAĞ

November 2006, 88 pages

The main objective of this study is to evaluate mixed mode stress intensity factors for inclined embedded cracks in functionally graded materials. Fracture analysis of inclined cracks requires the calculation of both Mode I and Mode II stress intensity factors (K_I, K_{II}). In this study, J_k-integral is used to calculate K_I and K_{II}. Equivalent domain integral approach is utilized to evaluate the J_k-integral around the crack tip. The present study aims at developing a finite element model to study inclined crack problems in graded media under thermomechanical loading. A two dimensional finite element model is developed for inclined cracks located in a functionally graded medium. Structural and thermal problems are solved using two dimensional finite elements namely 8-noded triangles. Material properties are sampled directly at the integration points of the elements, as required by the numerical integral evaluation. The main results of the study are the stress intensity factors at the crack tip for functionally graded materials subjected to thermomechanical loading.

Keywords: Functionally Graded Material, J_k-Integral, Inclined Cracks, Mixed-Mode Stress Intensity Factors

ÖZ

FONKSİYONEL DERECELENDİRİLMİŞ MALZEMELERDEKİ
EĞİK ÇATLAKLARIN ISIL GERİLME ŞİDDETİ FAKTÖRLERİNİN
J_k -INTEGRAL METODUYLA HESAPLANMASI

DEMİRÇİVİ, Bengi
Yüksek Lisans, Makina Mühendisliği Bölümü
Tez Yöneticisi : Asst. Prof. Dr. Serkan DAĞ

Kasım 2006, 88 sayfa

Bu çalışmanın temel amacı, fonksiyonel derecelendirilmiş malzemelerdeki gömülü eğik çatlakların karışık mod gerilme şiddeti faktörlerinin hesaplanmasıdır. Eğik çatlakların kırılma analizi, Mod I ve Mod II gerilme şiddeti faktörlerinin (K_I, K_{II}) hesaplanmasını gerektirir. Bu çalışmada, K_I ve K_{II} değerlerini hesaplamak için J_k -integrali kullanılmıştır. Çatlak ucundaki J_k -integrali eşdeğer alan integrali yaklaşımı kullanılarak hesaplanmıştır. Bu çalışma, mekanik yükleme altında fonksiyonel derecelendirilmiş malzemelerdeki eğik çatlak problemlerini incelemek için bir sonlu elemanlar modeli geliştirmeyi amaçlar. Fonksiyonel derecelendirilmiş ortamda eğik bir çatlak için iki boyutlu sonlu elemanlar modeli geliştirilmiştir. Yapısal ve ısısal problemler 8-nodlu üçgenler olan iki boyutlu sonlu elemanlarla modellenmiştir. Malzeme özellikleri, sayısal integral hesaplarının gerektirdiği gibi her bir elemanın tümleştirme noktalarında örneklenmiştir. Çalışmanın başlıca sonuçları, mekanik yükleme altında kalmış fonksiyonel derecelendirilmiş malzemeler için çatlak ucunda oluşan gerilme şiddeti faktörleridir.

Anahtar Kelimeler: Fonksiyonel Derecelendirilmiş Malzeme, J_k -Integrali, Eğik Çatlaklar, Karışık-Mod Gerilme Şiddeti Faktörleri

To My Darling

ACKNOWLEDGMENTS

The author wishes to express her gratitude to her supervisor Asst. Prof. Dr. Serkan DAĞ since he was the pioneer of this work. The author wishes to express her sincere appreciation to Assoc. Prof. Dr. Bora YILDIRIM who always oriented the author towards the correct direction.

This work wouldn't be done without the support of the author's altruistic parents Sema and Arif KARATEKİN and her only brother Tünay KARATEKİN.

The author wishes to thank her dear husband Fatih Levent DEMİRÇİVİ since he is the one half of the author's life and this thesis would not be completed without his presence.

The author is very grateful to her friends, Seda BAŞÖREN and her husband Behiç Barış ATEŞ for their splendid emotional support, Pınar and Harun KAYGAN for their relaxing friendships, Selcen and Ahmet KARCILAR for their hardware support, Pınar ŞAHİN for her warm friendship and Yavuz Selim KAYSERİLİOĞLU for his outstanding editing.

TABLE OF CONTENTS

LIST OF TABLES

LIST OF FIGURES

NOMENCLATURE

Latin Symbols

E	Modulus of Elasticity
J_k	J_k - Integral
K_I	Mode I stress intensity factor
K_{In}	Normalized Mode I stress intensity factor
K_{II}	Mode II stress intensity factor
K_{IIn}	Normalized Mode I stress intensity factor
n_i	Unit outward normal to the integration path
q	q function
T_s	T -stress
T_{sn}	Normalized T -stress
u_i	Displacement components
W	Mechanical strain energy density function
W^+	Mechanical strain energy density function at the upper crack face
W^-	Mechanical strain energy density function at the lower crack face
x_1	Crack tip coordinate x in indicial notation
x_2	Crack tip coordinate y in indicial notation

Greek Symbols

α	Thermal expansion coefficient
δ	Kronecker delta
ε_{ij}	Strain tensor
ϕ	Angle of crack
Γ	Line integral path

Ω	Domain integral area
σ_{ij}	Stress tensor
θ	Temperature difference
ν	Poisson's ratio

Subscripts

cr	Ceramic material property
m	Metallic material property

Superscripts

$+$	Upper crack surface
$-$	Lower crack surface

Abbreviations

DCT	Displacement Correlation Technique
EDI	Equivalent Domain Integral
FGM	Functionally Graded Material

CHAPTER 1

INTRODUCTION

1.1 Functionally Graded Materials

Materials science is developing to obtain the desired material property combinations for several engineering applications. Functionally Graded Materials (FGM's) are a good promise to meet the needs of engineering problems especially in severe environments. A functionally graded material is a multi-component composite characterized by a compositional gradient from one component to the other. In contrast, traditional composites are homogeneous mixtures and they therefore involve a compromise between the desirable properties of the component materials.

The FGM concept is originated in Japan during a space plane project in 1984, in the form of a proposed thermal barrier material capable of withstanding a surface temperature of 2000 K and a temperature gradient of 1000 K across a cross section less than 10 mm. Since 1984, FGM thin films have been comprehensively researched and are almost a commercial reality. FGM's were initially introduced to take the advantage of different properties of their constituents, since significant proportions of an FGM contain the pure form of each component and the need for decrease is eliminated. For example, the toughness of a metal can be mated with the refractoriness (heat and corrosion resistance) of a ceramic, without any compromise in the mechanical strength and toughness of the metal side or the refractoriness of the ceramic side. It is claimed by Kim and Paulino that, with such materials it can be possible to improve thermal or mechanical stress relaxation and to increase loading strength and toughness along coating / substrate interfaces [1].

In essence, FGM's are characterized by spatially varied microstructures created by non-uniform distributions of the reinforcement phase with different properties, sizes, shapes, as well as by interchanging the role of reinforcement and matrix materials in a continuous manner. Therefore, the volume fractions of the constituent materials of FGM's are varied continuously in a particular direction to create a certain type of material composition profile that is suitable for a given application. Consequently, these materials posses graded or continuously variable thermomechanical properties and the properties of both components can be fully utilized.

Scientific research on FGM's considers functions of gradients in materials comprising thermodynamic, mechanical, chemical, optical, electromagnetic, and/or biological aspects. FGM's offer solutions for applications where severe operating conditions occur. For example, wear-resistant linings for handling large, heavy abrasive ore particles, rocket heat shields, heat exchanger tubes, thermoelectric generators, heat-engine components, plasma facings for fusion reactors, and electrically insulating metal/ceramic joints. They are also ideal for minimizing thermomechanical mismatch in metal-ceramic bonding.

Recent advances in material processing have allowed manufacturing of wide diversity of FGM's. Large bulk FGM's can be produced by spark plasma sintering technique. FGM coatings can be manufactured by plasma spray or electron beam physical vapor deposition techniques. FGM coatings that are produced by these two methods can be modeled as orthotropic FGM's. However, FGM's which are produced by plasma sintering technique may be modeled as isotropic FGM's as presented by Kim and Paulino [2].

If properly used, such materials may also be used to reduce stress concentration or stress intensity factors. Stress response of FGM's differs substantially from those of their homogenous counterparts. For example, maximum stress is lower in an FGM than in a homogenous material in certain conditions [2].

1.2 Literature Survey

The fracture analyses can be carried out by employing several methods to calculate the stress intensity factors at the crack tips, such as stress-field theories, experimental techniques and *J*-integral. The *J*-integral is widely used in computational fracture mechanics analyses in order to evaluate stress intensity factors. In its generalized form, *J* is defined along a vanishingly small contour at a crack tip. This definition is known to be equivalent to the energy release rate for linear and nonlinear elastic materials. *J* can also be defined as a line integral over an arbitrary curve away from the crack tip under certain conditions. Rice presented that if the crack is in a homogenous medium subjected to mechanical loads and has traction free surfaces, *J* can be expressed as a path independent line integral [3].

If the crack is an inclined crack and/or in a functionally graded medium and/or subjected to thermal stresses, the generalized definition of *J* cannot be converted to a single path independent line integral. However, in these cases, it is possible to reduce *J* to a form that consists of line and domain integrals. Equivalent Domain Integral (EDI) approach is a systematic way of converting the generalized line integral definition of *J* to a domain independent form that contains both area and line integrals. By using the constitutive relations of plane isotropic thermoelasticity, the generalized definition of the *J*-integral is converted to an equivalent domain integral to calculate the thermal stress intensity factor. The EDI concept is previously explored to study crack problems in isotropic FGM's under mechanical loads by Gu *et al.* [4].

The path-independent J_k-integral is presented for FGM's considering plane elasticity by Kim and Paulino [1]. The formulation is a generalized procedure, since the crack orientation is arbitrary, not aligned with principal orthotropy directions. Equivalent domain integral approach is utilized for the calculation of

mixed-mode stress intensity factors and energy release rate. The performance of J_k-integral in computing mixed-mode stress intensity factors using a finite element method is examined in their study. The independent engineering constants such as elastic modulus, Poisson's ratio and shear parameter are exponentially and linearly varied for various problems. It is concluded that plate size, material property gradation (isotropy or orthotropy) and boundary conditions play a significant role in fracture behavior of FGM's. Numerical results show that Poisson's ratio plays a significant role for mixed-mode crack problems with prescribed boundary conditions; whereas it has a negligible effect for pure Mode I crack problems.

The effects of the material nonhomogeneity and orthotropy on fracture mechanics parameters are analyzed by Dağ *et al.* [5]. Analytical and computational techniques are focused on the cracks that are lying along an interface in a graded orthotropic medium. The authors argue that the Mode I stress intensity factor and energy release rate for an interface crack are monotonically decreasing functions of the coating stiffness of the functionally graded material. The results of this study show that for a single crack or for periodic cracks at the interface, the energy release rate is the decreasing function of the nonhomogeneity constant, β, and an increasing function of the shear parameter, κ, under uniform normal loading. The analytical approach constitutes of obtaining the general solution of governing partial differential equations for the graded orthotropic coating by means of Fourier transformations. The problem is modeled by means of 10-noded cubic triangular enriched finite elements. Enriched finite element utilization allows the direct calculation of SIF's and the need for post processing is reduced. Comparisons between the analytical approach and enriched finite element application conclude that the finite element solutions are within the range of $\pm 0.4\%$ of analytical results. It is claimed that this level of accuracy is hard to achieve when other means of finite element applications are utilized, such as Displacement Correlation Technique.

A study by Kim and Paulino [6] presents a general purpose formulation and finite element method implementation of mixed-mode crack problem for linearly elastic FGM's. This study utilizes Displacement Correlation Technique (DCT), Modified Crack Closure (MCC) and Equivalent Domain Integral (EDI) to calculate stress intensity factors. Exponentially varying material properties are implemented to the finite element codes. Specially designed crack tip elements that emanate from the crack tip region, are used for FEM and the effect of crack tip element size is also investigated in detail. Several numerical results obtained from three calculation methods are compared and it is concluded that EDI and MCC techniques are superior to DCT, especially for mixed-mode crack problems such as slanted edge crack. J_k-integral method is claimed to be sensitive to the choice of the size of the crack tip elements.

Graded finite elements which incorporate the material property gradient at the size scale of the element are utilized in the analysis of Kim and Paulino [7]. Using a generalized isoparametric formulation, performance of linear (Q4) and quadratic (Q8) elements are compared in different loading conditions, such as fixed grip, tension and bending. It is concluded that higher order elements (quadratic and higher) are superior to conventional homogenous elements based on the same shape functions. In order to investigate the influence of material properties on the stress response, linear and exponential variations of material properties are considered. Stress distribution of the exponentially varied material is smoother than the linearly varied material. It is concluded that graded elements provide a better approximation to the exact solution in every element.

A three dimensional finite element technique is used to examine the behavior of semi-elliptical surface cracks in FGM coatings by Yıldırım *et al.* [8]. A transient thermal analysis is conducted on the 3D model and it is observed that crack surfaces contact with each other after a certain period of time, that is, crack closure occurs. The time and location for the initiation of the crack closure is determined by finding out the point around the crack front and the time at which

the SIF becomes zero. SIF's are observed to go through a maximum as the FGM coating-substrate structure cools down from its initial temperature. It is concluded that a material property gradation in the coating can cause a decrease in the amplitude of Mode I SIF's under both mechanical and thermal loading.

For homogeneous materials, the fracture parameters such as K_I, K_{II} and T-stress depend on the geometry, size and external loading. FGM's possess material gradients through the layer which do not affect the order of singularity and the asymptotic angular functions which are presented in APPENDIX B. Paulino and Kim claimed that material gradients affect the fracture parameters [9]. T-stress has been extensively investigated for homogeneous materials. Larsson and Carlsson [10] investigated the T-stress in Mode I loading, and found that it affects the size and shape of the plastic zone and specimens with negative T-stress have lower constraint than those with positive T-stress. A stress substitution method is used to evaluate T-stress and T-stress is claimed to have a significant influence on crack initiation angles in brittle fracture of FGM's.

T-stress has also been shown to have a significant influence on crack-tip toughness of isotropic FGM's. Paulino and Kim [9] utilized the interaction integral approach to investigate the fracture behavior of FGM's with emphasis on the T-stress. It is concluded for both homogeneous and FGM cases that negative T-stress decreases the crack initiation angle, however positive T-stress increases the crack initiation angle. It is discussed that material gradation has a significant influence on the sign and magnitude of T-stress.

1.3 Scope of the Study

The aim of this study is to evaluate mixed mode stress intensity factors for inclined cracks in a functionally graded medium. A two dimensional finite element model is developed for this purpose using finite element software, ANSYS [11]. The path-independent J_k-integral is computed with the implementation of Equivalent Domain Integral method. EDI is implemented on the finite element model with the use of Gauss-Legendre Quadrature, a tool for the evaluation of integrals. The Gauss-Legendre Quadrature requires the integrand of the J_k-integral to be determined at each of the Gauss points. Therefore, subroutines are written in Ansys Parametric Design Language (APDL) to evaluate the required variables, such as stresses, strains, displacements and mechanical strain energy density function at the Gauss points of each element. An APDL subroutine is developed for the implementation of material property variations of FGM's. The material properties are specified for each element at its centroid. A circular domain is selected around the crack tip for simplicity. In this circular domain, the mesh is finely tuned in order to obtain more accurate results. 8-noded quadrilaterals are used to mesh the model. However, 8-noded quadrilaterals are modeled such that three nodes share the same node number. Therefore, 8-noded triangular elements with same properties as quadrilaterals are used in finite element models. Furthermore, in order to simulate the stress concentration at the crack tip more accurately in DCT subroutines, the mesh is skewed at the crack tip and the 8-noded quadrilaterals are collapsed to triangles around the crack tip. After the J_k-integral is evaluated, the relation between mixed mode SIF's and J_k-integral is used in another APDL subroutine to compute SIF's. The model is subjected to thermal loads. In the previously determined time range, the reaction of the model at all of the time steps is analyzed. In order to examine the accuracy of the model, calculated SIF's are compared with those available in the literature.

This thesis contains six chapters. An introduction, literature survey and the scope of the study are given in the present chapter. In Chapter 2, theories of elasticity and fracture are explained in detail. The two dimensional inclined crack problem is defined in Chapter 3. The details of the finite element modeling and the application of Equivalent Domain Integral (EDI) method are given in Chapter 4. The computed results and discussions are presented in Chapter 5. Finally, concluding remarks are given in Chapter 6.

CHAPTER 2

FORMULATION OF J_k -INTEGRAL

2.1 Theory of Elasticity

Theory of elasticity focuses on the internal response of a continuous homogenous body to the action of external forces. This hypothetical body, illustrated in Figure 2.1 is assumed to be in static equilibrium.

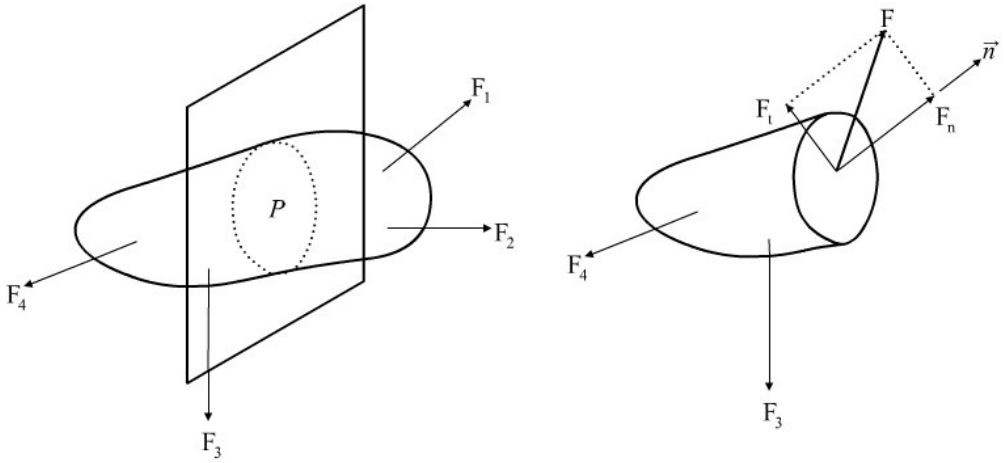

Figure 2.1 Equilibrium of an arbitrary body.

Using Newton's principle of action and reaction , one can imagine that the body is cut by a fictitious plane passing through a point *P*, within the body and the removed portion is replaced by an equivalent force, *F*, acting on the cross-sectional area, *A*, as shown in Figure 2.1. This force has the magnitude and direction needed to restore static equilibrium to the remaining portion of the body. Further, one can resolve *F* into components normal to the plane, F_n, and

tangential to the plane, F_t. The concept of stress at a point is obtained by shrinking the area, A, to infinitesimal dimensions.

Formally, the normal stress, σ and the shear stress, τ are defined as

$$\sigma = \lim_{A \to 0} \frac{|F_n|}{A} \qquad \tau = \lim_{A \to 0} \frac{|F_t|}{A} \qquad \textbf{(2.1.a, b)}$$

Clearly, σ and τ depend on the orientation of the plane passing through *P* and vary from point to point.

A complete description of the stresses acting at a point can be obtained by constructing a Cartesian coordinate system at the point and examining the average forces per unit area acting on the faces of an infinitesimally small cube surrounding the point. Using the definition of normal and shear stresses from (2.1), the stresses on each face can be represented in Cartesian form, as shown in Figure 2.2.

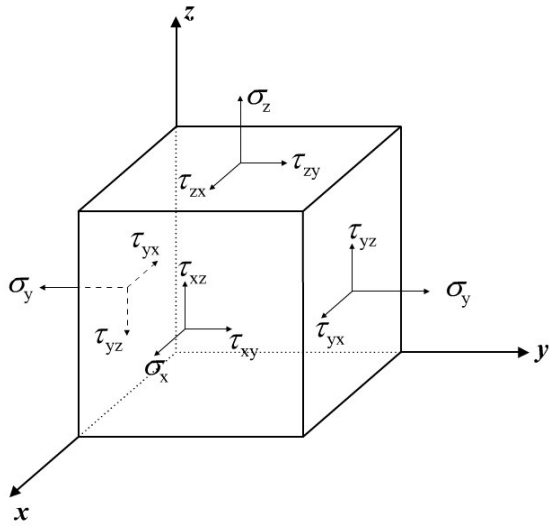

Figure 2.2 Cartesian components of stress in three dimensions

If the stresses are slowly varying across the infinitesimal cube, moment equilibrium about the centroid of the cube requires that,

$$\tau_{xy} = \tau_{yx} \qquad \tau_{xz} = \tau_{zx} \qquad \tau_{zy} = \tau_{yz} \tag{2.2}$$

As a result, the nine stress components depicted in Figure 2.2 reduce to six independent quantities that one can write in an array, called stress tensor, as follows

$$\sigma_{ij} = \begin{bmatrix} \sigma_x & \tau_{xy} & \tau_{xz} \\ \tau_{xy} & \sigma_y & \tau_{yz} \\ \tau_{xz} & \tau_{yz} & \sigma_z \end{bmatrix} \tag{2.3}$$

where, σ_{ij} is the stress components expressed in indicial notation.

Stress tensor is the outcome of the action of forces on the infinitesimal cube. When the distortion of the infinitesimally small cube is considered, the measure of distortion, called *state of strain* is introduced. The state of strain is described in terms of the displacements of the point from its undistorted position and its derivatives. In the Cartesian coordinate system, the displacements in the coordinate dimensions *x, y* and z are defined as *u, v* and *w*, respectively. Then, for small displacements in a continuous body, the strains in terms of the displacement gradients are given by

$$\varepsilon_x = \frac{\partial u}{\partial x} \qquad \varepsilon_y = \frac{\partial v}{\partial y} \qquad \varepsilon_z = \frac{\partial w}{\partial z}$$

$$\gamma_{xy} = \frac{\partial u}{\partial y} + \frac{\partial v}{\partial x} \qquad \gamma_{xz} = \frac{\partial u}{\partial z} + \frac{\partial w}{\partial x} \qquad \gamma_{yz} = \frac{\partial v}{\partial z} + \frac{\partial w}{\partial y} \tag{2.4.a-f}$$

The strain tensor is defined as

$$\varepsilon_{ij} = \frac{1}{2}\left(\frac{\partial u_i}{\partial x_j} + \frac{\partial u_j}{\partial x_i} \right) = \begin{bmatrix} \varepsilon_x & \frac{\gamma_{xy}}{2} & \frac{\gamma_{xz}}{2} \\ \frac{\gamma_{xy}}{2} & \varepsilon_y & \frac{\gamma_{yz}}{2} \\ \frac{\gamma_{xz}}{2} & \frac{\gamma_{yz}}{2} & \varepsilon_z \end{bmatrix} \quad \textbf{(2.5)}$$

Stress is a conceptual quantity related to the force acting at a point. It is assumed that a material medium exists such that the stress acts against some resistance. Similarly, strain is a kinematic quantity relating relative motion between points in a material medium.The definitions of both stress and strain tensors are independent of material medium in which they act. The relation between state of stress and state of strain is called the *constitutive equation*. The material is assumed to be isotropic and homogenous. However, this study concentrates on FGM's for which material properties vary from point to point by a function. The material properties for FGM's are sampled for every single point and the constitutive relations given below are applied for each of the points.

Lame's constants are introduced as follows,

$$\beta = \frac{\alpha E}{1 - 2\upsilon} \qquad \lambda = \frac{\upsilon E}{(1+\upsilon)(1-2\upsilon)} \qquad \mu = \frac{E}{2(1+\upsilon)} \quad \textbf{(2.6)}$$

where, E is modulus of elasticity of the material

υ is Poisson's ratio of the material.

The temperature difference is defined as,

$$\theta = \Delta T = T - T_{initial} \quad \textbf{(2.7)}$$

Introducing the Kronecker Delta for indicial notation;

$$\delta_{ij} = \begin{cases} 1 & if \quad i = j \\ 0 & if \quad i \neq j \end{cases} \quad \textbf{(2.8)}$$

For a general 3D state of stress, constitutive relation for thermal analysis can be written as follows,

$$\sigma_{ij} = 2\mu\varepsilon_{ij} + \lambda\varepsilon_{kk}\delta_{ij} - \beta\theta\delta_{ij} \quad \textbf{(2.9)}$$

The equations of motion that constitute the *kinetics* of the problem is obtained by analyzing the equilibrium conditions of the infinitesimal cube of Figure 2.2 and are given in indicial notation by

$$\sigma_{ij,j} + B_i = \rho\frac{\partial^2 u_i}{\partial t^2} \quad \textbf{(2.10)}$$

where, $\sigma_{ij,j}$ is the derivatives of stress tensor

B_i is the body forces

u_i is the displacements in indicial notation.

In the absence of body forces and for the static case, (2.10) reduces to

$$\sigma_{ij,j} = 0 \quad \textbf{(2.11)}$$

There are two special cases in which the anti-plane behavior is restricted and the governing equations of elasticity can be formulated in two dimensions.

State of Plane Strain: All anti-plane strains are zero.

$$\varepsilon_z = 0 \qquad \gamma_{xz} = 0 \qquad \gamma_{yz} = 0 \quad \textbf{(2.12)}$$

State of Plane Stress: All anti-plane stresses are zero.

$$\sigma_z = 0 \qquad \tau_{xz} = 0 \qquad \tau_{yz} = 0 \quad \textbf{(2.13)}$$

2.2 Fracture Mechanics Theory

Theory of fracture mechanics focuses on failure of structures containing cracks based on some calculation methods. All of these methods are developed for the derivation of Stress Intensity Factors (SIF's). An accurate prediction of stress intensity factors at crack tips is essential for assessing the strength and life of structures using fracture mechanics theories. The methods for extracting stress intensity factors from computed displacement solutions fall into two categories; displacement matching methods and energy based methods.

Displacement matching methods assumes a form of the local solution and the value of the displacement near crack tip is used to determine the magnitude of the coefficients in the asymptotic expansion.

Energy based methods relate the strength of the singular stress field to the energy release rate, i.e. the sensitivity of the total potential energy to the crack position. An expression for calculating the energy release rate in two dimensional cracks is given by Rice [3] and is known as the *J*-integral. The *J*-integral is a path independent contour integral involving the projection of the material force derived from Eshelby's [12] energy momentum tensor along the direction of the possible crack extension. An alternative form of the *J*-integral is transformed into a domain integral, namely, J_k-integral.

2.2.1 J_k -Integral Formulation

Consider a loop Γ_ε around the crack tip as shown in Figure 2.3;

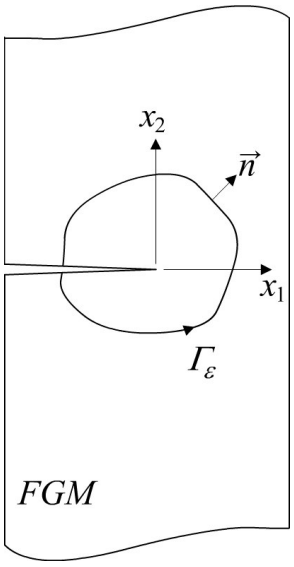

Figure 2.3 Schematic of a J_k -integral path around the crack tip.

Equivalent Domain Integral approach is a systematic way of converting the generalized line integral definition of J -integral to a domain independent form that contains only area integrals. By using this method, domain independent integrals can be derived for FGM's subjected to thermal stresses.

The generalized J -integral is converted to an area integral by carrying out the necessary modifications resulting from material property gradation and thermal strains [13].

The path independent line integral, J_k is defined in the following form [14]:

$$J_k = \lim_{\Gamma_\varepsilon \to 0} \int_{\Gamma_\varepsilon} \left(W n_k - \sigma_{ij} n_j u_{i,k} \right) d\Gamma \tag{2.14}$$

where, W is the mechanical strain energy density function,

n_k is the unit outward normal to Γ_ε,

σ_{ij} are the stress components,

$i,j,k = 1, 2, 3$

This form of formulation is not suitable for numerical analysis, since it is not feasible to evaluate stresses and strains along a vanishingly small contour. A convenient approach in the finite element implementation of the J_k-integral is to convert the generalized line integral definition to an equivalent domain integral (EDI) calculated around the crack tip.

To define the equivalent domain integral, one should define an area Ω around the crack tip as shown in Figure 2.4.

The integration path is the addition of four paths around the crack tip;

$$\Gamma = \Gamma_0 + \Gamma_C^+ + \Gamma_C^- + \Gamma_\varepsilon \tag{2.15}$$

and the integration area is introduced as;

$$\Omega = \Omega_0 - \Omega_\varepsilon \tag{2.16}$$

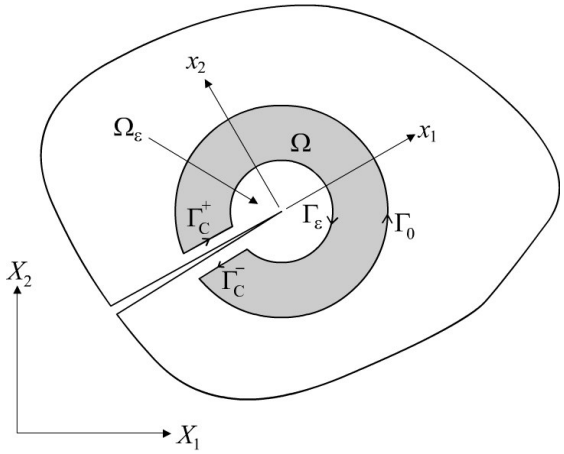

Figure 2.4 J_k-integral integration path.

A piecewise smooth function, q is introduced as follows(APPENDIX C);

$$q = \begin{cases} 0 \;\; on \;\; \Gamma_0 \\ 1 \;\; on \;\; \Gamma_\varepsilon \end{cases} \tag{2.17}$$

Now, let us consider the line integral;

$$\oint_{\Gamma} \left(\sigma_{ij} n_j u_{i,k} - W n_k \right) q \, d\Gamma \tag{2.18}$$

Utilizing the Kronecker Delta, one can write;

$$n_k = \delta_{kj} n_j \tag{2.19}$$

Combining (2.18) with (2.19),

$$I_k = \oint \left(\sigma_{ij} u_{i,k} q - W \delta_{kj} q \right) n_j \, d\Gamma \tag{2.20}$$

By utilizing the divergence theorem (APPENDIX A) in the plane, the line integral is converted to a domain integral.

$$I_k = \oint_{\Gamma} \left(\sigma_{ij} u_{i,k} q - W \delta_{kj} q \right) n_j \, d\Gamma = \iint_{\Omega} \frac{\partial}{\partial x_j} \left(\sigma_{ij} u_{i,k} q - W \delta_{kj} q \right) d\Omega \tag{2.21}$$

Concentrating on the integrand of the domain integral;

$$S = \frac{\partial}{\partial x_j} \left(\sigma_{ij} u_{i,k} - W \delta_{kj} \right) q \tag{2.22}$$

Differentiating the terms with respect to x_j ,

$$S = \left(\sigma_{ij,j} u_{i,k} + \sigma_{ij} u_{i,kj} - W_{,j} \delta_{kj} - W \delta_{kj,j} \right) q + \left(\sigma_{ij} u_{i,k} - W \delta_{kj} \right) q_{,j} \tag{2.23}$$

Kronecker Delta has the properties of,

$$\delta_{kj,j} = 0 \qquad\qquad W_{,j} \delta_{kj} = W_{,k} \tag{2.24.a, b}$$

Combining (2.23) with (2.24.a ,b)

$$S = \underbrace{\left(\sigma_{ij,j} u_{i,k} + \sigma_{ij} u_{i,kj} - W_{,k} \right) q}_{\text{First Term, } S_1} + \underbrace{\left(\sigma_{ij} u_{i,k} - W \delta_{kj} \right) q_{,j}}_{\text{Second Term, } S_2} \tag{2.25}$$

Concentrating on the terms of S_1,

$$S_1 = \left(\sigma_{ij,j} u_{i,k} + \sigma_{ij} u_{i,kj} - W_{,k} \right) q \tag{2.26}$$

$$W_{,k} = \frac{\partial W}{\partial x_k} = \frac{\partial W}{\partial \varepsilon_{ij}} \frac{\partial \varepsilon_{ij}}{\partial x_k} + \left(\frac{\partial W}{\partial x_k} \right)_{\text{expl}} \tag{2.27}$$

$\left(\frac{\partial W}{\partial x_k} \right)_{\text{expl}}$ is the explicit derivative of W and defined as, [14]

$$\left(\frac{\partial W}{\partial x_k} \right)_{\text{expl}} = \frac{\partial W}{\partial \mu} \frac{\partial \mu}{\partial x_k} + \frac{\partial W}{\partial \lambda} \frac{\partial \lambda}{\partial x_k} + \frac{\partial W}{\partial \beta} \frac{\partial \beta}{\partial x_k} + \frac{\partial W}{\partial \alpha} \frac{\partial \alpha}{\partial x_k} + \frac{\partial W}{\partial \theta} \frac{\partial \theta}{\partial x_k} \tag{2.28}$$

The definition of mechanical strain energy density function suggests that,

$$\frac{\partial W}{\partial \varepsilon_{ij}} = \sigma_{ij} \tag{2.29}$$

Substituting (2.29) into (2.27) the following is obtained in indicial notation,

$$W_{,k} = \sigma_{ij}\, \varepsilon_{ij,k} + \left(W_{,k} \right)_{\text{expl}} \tag{2.30}$$

Differentiating (2.5) with respect to k and substituting into (2.30),

$$W_{,k} = \sigma_{ij} \frac{1}{2} \frac{\partial}{\partial x_k} \left(\frac{\partial u_i}{\partial x_j} + \frac{\partial u_j}{\partial x_i} \right) + \left(W_{,k} \right)_{\text{expl}} \tag{2.31}$$

$$W_{,k} = \frac{1}{2} \sigma_{ij} \frac{\partial^2 u_i}{\partial x_k \partial x_j} + \frac{1}{2} \sigma_{ij} \frac{\partial^2 u_j}{\partial x_k \partial x_i} + \left(W_{,k} \right)_{\text{expl}} \tag{2.32}$$

At this stage, one should interchange the dummy indices of the second term to simplify the equation. After necessary simplifications, one can obtain the following,[14]

$$W_{,k} = \sigma_{ij}\, u_{i,kj} + \left(W_{,k} \right)_{\text{expl}} \tag{2.33}$$

Substituting (2.33) in (2.26),

$$S_1 = \sigma_{ij,j}\, u_{i,k} - \left(W_{,k} \right)_{\text{expl}} \tag{2.34}$$

Using (2.11),

$$\sigma_{ij,j} = 0 \tag{2.35}$$

(2.34) reduces to,

$$S_1 = -\left(W_{,k} \right)_{\text{expl}} \tag{2.36}$$

As a result, the integrand of the domain integral can be written as follows,

$$S = -\left(W_{,k} \right)_{\text{expl}} q + \left(\sigma_{ij}\, u_{i,k} - W\, \delta_{kj} \right) q_{,j} \tag{2.37}$$

Hence, (2.21) can be written as follows,

$$I_k = \int_{\Gamma} \left(\sigma_{ij}\, u_{i,k}\, q - W\, \delta_{kj}\, q \right) n_j \, d\Gamma = \iint_{\Omega} \frac{\partial}{\partial x_j} \left(\sigma_{ij}\, u_{i,k} \; - W\, \delta_{kj} \right) q_{,j} \, d\Omega - \iint_{\Omega} \left(W_{,k} \right)_{\text{expl}} q \, d\Omega \quad \textbf{(2.38)}$$

Considering the line integral on Γ,

$$\left(\sigma_{ij}\, u_{i,k} \; - W\, \delta_{kj} \right) q\, n_j = b_k \quad \textbf{(2.39)}$$

Taking the line integral of both sides of (2.15)

$$I_k = \int_{\Gamma} b_k d\Gamma = \int_{\Gamma_\varepsilon} b_k d\Gamma + \int_{\Gamma_C^+} b_k d\Gamma + \int_{\Gamma_C^-} b_k d\Gamma + \int_{\Gamma_0} b_k d\Gamma \quad \textbf{(2.40)}$$

The change of the orientation of Γ_ε curve can be observed in Figure 2.5.

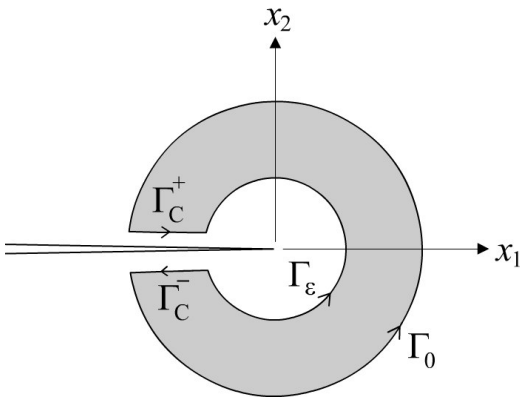

Figure 2.5 Re-orientation of the integration curves

Since the *q*-function has a value of zero on Γ_0, $b_k = 0$ on this curve. Substituting this fact and the re-orientation effects on (2.40), one can obtain,

$$I_k = \int_{\Gamma} b_k \, d\Gamma = - \int_{\Gamma_{\varepsilon,new}} b_k \, d\Gamma + \int_{\Gamma_C^+} b_k \, d\Gamma + \int_{\Gamma_C^-} b_k \, d\Gamma \quad \textbf{(2.41)}$$

Substituting (2.39) in the line integral of the newly oriented curve,

$$\int_{\Gamma} b_k \, d\Gamma = \underbrace{\int_{\Gamma_{\varepsilon,new}} \left(W\, \delta_{kj} - \sigma_{ij}\, u_{i,k} \right) q\, n_j \, d\Gamma}_{J_k} + \int_{\Gamma_C^+} b_k \, d\Gamma + \int_{\Gamma_C^-} b_k \, d\Gamma \quad \textbf{(2.42)}$$

Keeping in mind that $\Omega = \Omega_0 - \Omega_\varepsilon$ and taking the limit as $\Gamma_\varepsilon \to 0$, and substituting (2.38) into (2.42) the following is obtained,

$$J_k = \iint_{\Omega} \left(\sigma_{ij}\, u_{i,k} - W\,\delta_{kj}\right) q_{,j}\, d\Omega - \iint_{\Omega} \left(W_{,k}\right)_{\text{expl}} q\, d\Omega - \int_{\Gamma_C^+} \left(\sigma_{ij}\, u_{i,k} - W\,\delta_{kj}\right) q\, n_j\, d\Gamma - \int_{\Gamma_C^-} \left(\sigma_{ij}\, u_{i,k} - W\,\delta_{kj}\right) q\, n_j\, d\Gamma \tag{2.43}$$

Concentrating on the terms of line integrals on Γ_C^+ and Γ_C^-, it is observed that displacement derivatives with respect to *k* equals zero on these curves, therefore

$$\sigma_{ij}\, u_{i,k}\, n_j = 0 \tag{2.44}$$

Substituting (2.44) into (2.43),

$$J_k = \iint_{\Omega} \left(\sigma_{ij}\, u_{i,k} - W\,\delta_{kj}\right) q_{,j}\, d\Omega - \iint_{\Omega} \left(W_{,k}\right)_{\text{expl}} q\, d\Omega + \int_{\Gamma_C^+} W^+ n_k^+\, q\, d\Gamma + \int_{\Gamma_C^-} W^- n_k^-\, q\, d\Gamma \tag{2.45}$$

Let us combine the two terms which involve integrations along two crack faces Γ_C^+ and Γ_C^- and define Γ_C, the associated path of integration. The orientation of the curve can be changed and the corresponding normal for the integral can be evaluated on curve Γ_C^-. So, both integrals are evaluated over the same horizontal line. The path of integration can be denoted as Γ_C. Therefore, the integral becomes;

$$J_k = \iint_{\Omega} \left(\sigma_{ij}\, u_{i,k} - W\,\delta_{kj}\right) q_{,j}\, d\Omega - \iint_{\Omega} \left(W_{,k}\right)_{\text{expl}} q\, d\Omega + \int_{\Gamma_C} \left(W^+ - W^-\right) n_k^+\, q\, d\Gamma \tag{2.46}$$

where, the notation of $\left(W^+ - W^-\right)$ denotes the discontinuity (or jump) in the mechanical strain energy density across crack faces [1].

J_k - integral can be separated into Mode I and Mode II contributions as follows,

$$J_1 = \iint_{\Omega} \left(\sigma_{ij}\, u_{i,1} - W\,\delta_{1j}\right) q_{,j}\, d\Omega - \iint_{\Omega} \left(W_{,1}\right)_{\text{expl}} q\, d\Omega \tag{2.47.a}$$

$$J_2 = \iint_{\Omega} \left(\sigma_{ij}\, u_{i,2} - W\,\delta_{2j}\right) q_{,j}\, d\Omega - \iint_{\Omega} \left(W_{,2}\right)_{\text{expl}} q\, d\Omega + \int_{\Gamma_C} \left(W^+ - W^-\right) n_2^+\, q\, d\Gamma \tag{2.47.b}$$

It can be observed that J_1 term does not have a line integral term. This is due to the fact that, $n_1^+ = 0$ on both curves, Γ_C^+ and Γ_C^-.

2.2.2 J_1-Integral Formulation

Re-organizing the equation (2.47.a);

$$J_1 = \iint_{\Omega} \left(\sigma_{ij}\, u_{i,1}\, q_{,j} - W\, \delta_{1j}\, q_{,j} \right) d\Omega - \iint_{\Omega} \left(W_{,1} \right)_{\text{expl}} q\, d\Omega \qquad \textbf{(2.48)}$$

The term W is the mechanical strain energy density function and is defined as,[14]

$$W = \frac{1}{2} \sigma_{ij}\, \varepsilon_{ij}^{m} \qquad \textbf{(2.49)}$$

where ε_{ij}^{m} is the mechanical strain and defined as

$$\varepsilon_{ij}^{m} = \varepsilon_{ij} - \alpha \theta\, \delta_{ij} \qquad \textbf{(2.50)}$$

where θ is the temperature difference

Substituting (2.9) and (2.50) into (2.49) one can obtain

$$W = \mu\, \varepsilon_{ij}\, \varepsilon_{ij} + \frac{\lambda}{2} \varepsilon_{kk}^{2} - \beta \theta\, \varepsilon_{kk} + \frac{3}{2} \beta \alpha \theta^{2} \qquad \textbf{(2.51)}$$

The explicit derivative of mechanical strain energy density function is expressed as,

$$\left(W_{,1} \right)_{\text{expl}} = \left(\frac{\partial W}{\partial x_1} \right)_{\text{expl}} = \frac{\partial W}{\partial \mu} \frac{\partial \mu}{\partial x_1} + \frac{\partial W}{\partial \lambda} \frac{\partial \lambda}{\partial x_1} + \frac{\partial W}{\partial \beta} \frac{\partial \beta}{\partial x_1} + \frac{\partial W}{\partial \alpha} \frac{\partial \alpha}{\partial x_1} + \frac{\partial W}{\partial \theta} \frac{\partial \theta}{\partial x_1} \qquad \textbf{(2.52)}$$

Explicitly expressing the indicial notation of terms for plane strain condition,

$$\sigma_{ij}\, u_{i,1}\, q_{,j} = \sigma_{11}\, u_{1,1}\, q_{,1} + \sigma_{21}\, u_{2,1}\, q_{,1} + \sigma_{12}\, u_{1,1}\, q_{,2} + \sigma_{22}\, u_{2,1}\, q_{,2} \qquad \textbf{(2.53)}$$

and

$$W = \mu \left(\varepsilon_{11}^{2} + 2\varepsilon_{12}^{2} + \varepsilon_{22}^{2} \right) + \frac{\lambda}{2} \left(\varepsilon_{11} + \varepsilon_{22} \right)^{2} - \beta \theta \left(\varepsilon_{11} + \varepsilon_{22} \right) + \frac{3}{2} \beta \alpha \theta^{2} \qquad \textbf{(2.54)}$$

then partial derivatives can be found as follows [14]

$$\frac{\partial W}{\partial \mu} = F_{\mu} = \left(\varepsilon_{11}^{2} + 2\varepsilon_{12}^{2} + \varepsilon_{22}^{2} \right)$$

$$\frac{\partial W}{\partial \lambda} = F_{\lambda} = \frac{1}{2} \left(\varepsilon_{11} + \varepsilon_{22} \right)^{2}$$

$$\frac{\partial W}{\partial \beta} = F_{\beta} = \frac{3}{2}\alpha\theta^2 - \theta(\varepsilon_{11} + \varepsilon_{22})$$

$$\frac{\partial W}{\partial \alpha} = F_{\alpha} = \frac{3}{2}\beta\theta^2$$

$$\frac{\partial W}{\partial \theta} = F_{\theta} = 3\beta\alpha\theta - \beta(\varepsilon_{11} + \varepsilon_{22}) \qquad \textbf{(2.55.a-e)}$$

The terms $\frac{\partial \mu}{\partial x_1}, \frac{\partial \lambda}{\partial x_1}, \frac{\partial \beta}{\partial x_1}, \frac{\partial \alpha}{\partial x_1}$ are the derivatives of material properties and $\frac{\partial \theta}{\partial x_1}$ is the derivative of temperature difference with respect to x_1.

2.2.3 J_2-Integral Formulation

Re-organizing the equation (2.47.b);

$$J_2 = \iint_{\Omega} \left(\sigma_{ij}\, u_{i,2}\, q_{,j} - W\, \delta_{2j}\, q_{,j} \right) d\Omega - \iint_{\Omega} \left(W_{,2} \right)_{\text{expl}} q\, d\Omega + \int_{\Gamma_c} \left(W^{+} - W^{-} \right) n_2^{+}\, q\, d\Gamma \quad \textbf{(2.56)}$$

Keeping in mind that (2.49) is still valid, the explicit derivative of mechanical strain energy density function is expressed as,

$$\left(W_{,2} \right)_{\text{expl}} = \left(\frac{\partial W}{\partial x_2} \right)_{\text{expl}} = \frac{\partial W}{\partial \mu}\frac{\partial \mu}{\partial x_2} + \frac{\partial W}{\partial \lambda}\frac{\partial \lambda}{\partial x_2} + \frac{\partial W}{\partial \beta}\frac{\partial \beta}{\partial x_2} + \frac{\partial W}{\partial \alpha}\frac{\partial \alpha}{\partial x_2} + \frac{\partial W}{\partial \theta}\frac{\partial \theta}{\partial x_2} \quad \textbf{(2.57)}$$

Explicitly expressing the indicial notation of terms for plane strain condition,

$$\sigma_{ij}\, u_{i,2}\, q_{,j} = \sigma_{11}\, u_{1,2}\, q_{,1} + \sigma_{21}\, u_{2,2}\, q_{,1} + \sigma_{12}\, u_{1,2}\, q_{,2} + \sigma_{22}\, u_{2,2}\, q_{,2} \quad \textbf{(2.58)}$$

Equations (2.54) and (2.55) are also valid for this integral.

Concentrating on the $\int_{\Gamma_c} \left(W^{+} - W^{-} \right) n_2^{+}\, q\, d\Gamma$ term of J_2-integral, which is the integration along the crack faces of discontinuity in mechanical strain energy density as shown in Figure 2.6.

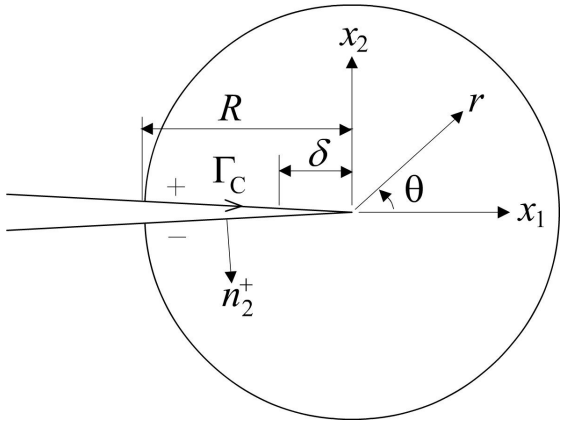

Figure 2.6 Schematic of the line integral $\int_{\Gamma_c} \left(W^{+} - W^{-} \right) n_2^{+}\, q\, d\Gamma$

At this point, the mechanical strain energy density function in terms of stress components is required.

$$W = \frac{1}{4\mu}\sigma_{ij}\,\sigma_{ij} - \frac{\lambda}{4\mu(3\lambda+2\mu)}\sigma_{kk}^2 \qquad \textbf{(2.59)}$$

For plane strain case, the explicit form of mechanical strain energy density function is as follows,

$$W = \frac{1}{4\mu}\left(\sigma_{11}^2 + 2\sigma_{12}^2 + \sigma_{22}^2 + \sigma_{33}^2\right) - \frac{\lambda}{4\mu(3\lambda+2\mu)}\left(\sigma_{11}+\sigma_{22}+\sigma_{33}\right)^2 \qquad \textbf{(2.60)}$$

For plane stress case, the explicit form of mechanical strain energy density function is as follows,

$$W = \frac{1}{4\mu}\left(\sigma_{11}^2 + 2\sigma_{12}^2 + \sigma_{22}^2\right) - \frac{\lambda}{4\mu(3\lambda+2\mu)}\left(\sigma_{11}+\sigma_{22}\right)^2 \qquad \textbf{(2.61)}$$

Note that the integrand of the line integral can be written as,

$$\left(W^+ - W^-\right) = W(r,\pi) - W(r,-\pi) \qquad \textbf{(2.62)}$$

This term can be calculated by utilizing the asymptotic expressions for stress components near the crack tip. (APPENDIX B)

When (B.1) equations are substituted into (2.62), one can obtain the following

$$\left(W^+ - W^-\right) = -\frac{4K_{II}T_s}{E'\sqrt{2\pi R}} \qquad \textbf{(2.63)}$$

where T_s is the nonsingular stress, or *T*-stress

$$E' = \begin{cases} E_{tip} & \text{, plane stress} \\ E_{tip} \Big/ \left(1-\upsilon_{tip}^2\right) & \text{, plane strain} \end{cases} \qquad \textbf{(2.64)}$$

$$\int_{\Gamma_C}\left(W^+ - W^-\right)n_2^+\,q\,d\Gamma = -\int_0^{R-\delta}\left(W^+ - W^-\right)\frac{x}{R}dx + \int_{R-\delta}^{R}\frac{4K_{II}T_s}{E'\sqrt{2\pi r}}\frac{x}{R}dx \qquad \textbf{(2.65)}$$

where, $n_2^+ = -1$, unit normal to Γ_C curve as shown in Figure 2.6

$q = \frac{x}{R}$, q function (APPENDIX C)

The line integral, $\int_{\Gamma_c} \left(W^+ - W^-\right) n_2^+ \, q \, d\Gamma$ is divided into two parts in (2.65). The first term is calculated numerically and second term is evaluated analytically. The values of δ should be sufficiently small so that asymptotic representations can be used for stress components. Taking small values for δ also makes it feasible to assume the material properties to be constant for those small distances and equal to the crack tip material properties.

Integrating the second term of (2.65), [14]

$$\int_{\Gamma_c} \left(W^+ - W^-\right) n_2^+ \, q \, d\Gamma = -\int_0^{R-\delta} \left(W^+ - W^-\right) \frac{x}{R} dx + \sqrt{\frac{\delta}{2\pi}} \frac{8 K_{II} T_s \left(3R - \delta\right)}{3 E' R} \qquad \textbf{(2.66)}$$

Substituting (2.66) into (2.56),

$$\begin{aligned} J_2 = \iint_{\Omega} \left(\sigma_{ij} u_{i,2} \, q_{,j} - W \delta_{2j} \, q_{,j}\right) d\Omega - \iint_{\Omega} \left(W_{,2}\right)_{\text{expl}} q \, d\Omega \\ - \int_0^{R-\delta} \left(W^+ - W^-\right) \frac{x}{R} dx + \sqrt{\frac{\delta}{2\pi}} \frac{8 K_{II} T_s \left(3R - \delta\right)}{3 E' R} \end{aligned} \qquad \textbf{(2.67)}$$

2.2.4 Stress Intensity Factor Calculation

Rewriting (2.47) and (2.67)

$$J_1 = \iint_{\Omega} \left(\sigma_{ij}\, u_{i,1}\, q_{,j} - W\, \delta_{1j}\, q_{,j}\right) d\Omega - \iint_{\Omega} \left(W_{,1}\right)_{\text{expl}} q\, d\Omega \tag{2.68.a}$$

$$\begin{aligned} J_2 = \iint_{\Omega} \left(\sigma_{ij}\, u_{i,2}\, q_{,j} - W\, \delta_{2j}\, q_{,j}\right) d\Omega - \iint_{\Omega} \left(W_{,2}\right)_{\text{expl}} q\, d\Omega \\ - \int_{0}^{R-\delta} \left(W^{+} - W^{-}\right) \frac{x}{R} dx + \sqrt{\frac{\delta}{2\pi}}\, \frac{8\, K_{II}\, T_s \left(3R - \delta\right)}{3\, E' R} \end{aligned} \tag{2.68.b}$$

The relation between J_1 , J_2 and stress intensity factors K_I , K_{II} is given by, [6]

$$J_1 = \frac{K_I^2 + K_{II}^2}{E'} \tag{2.69.a}$$

$$J_2 = -\frac{2\, K_I\, K_{II}}{E'} \tag{2.69.b}$$

A new quantity, $\hat{J}_2$ is introduced

$$\hat{J}_2 = \iint_{\Omega} \left(\sigma_{ij}\, u_{i,2}\, q_{,j} - W\, \delta_{2j}\, q_{,j}\right) d\Omega - \iint_{\Omega} \left(W_{,2}\right)_{\text{expl}} q\, d\Omega - \int_{0}^{R-\delta} \left(W^{+} - W^{-}\right) \frac{x}{R} dx \tag{2.70}$$

Substituting this new quantity in (2.68.b)

$$\hat{J}_2 + \sqrt{\frac{\delta}{2\pi}}\, \frac{8\, K_{II}\, T_s \left(3R - \delta\right)}{3\, E' R} = -\frac{2\, K_I\, K_{II}}{E'} \tag{2.71}$$

The quantity $\hat{J}_2$ is computed numerically on a given domain for two values of δ, namely δ_1 and δ_2 as shown in Figure 2.7.

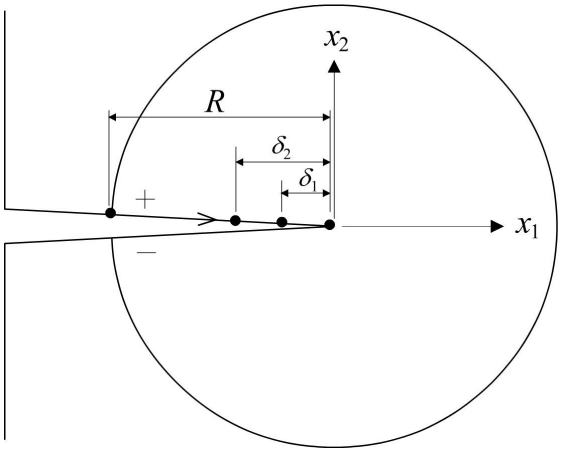

Figure 2.7 Line integral paths for upper and lower crack faces

When δ_1 and δ_2 are substituted into (2.71), $\hat{J}_2^1$ and $\hat{J}_2^2$ are obtained.

$$\hat{J}_2^1 = -\frac{2K_I K_{II}}{E'} - \sqrt{\frac{\delta_1}{2\pi}}\,\frac{8K_{II}T_s\left(3R-\delta_1\right)}{3E'R} \qquad \textbf{(2.72.a)}$$

$$\hat{J}_2^2 = -\frac{2K_I K_{II}}{E'} - \sqrt{\frac{\delta_2}{2\pi}}\,\frac{8K_{II}T_s\left(3R-\delta_2\right)}{3E'R} \qquad \textbf{(2.72.b)}$$

Let

$$G = -\frac{8K_{II}T_s}{\sqrt{2\pi}\,E'} \qquad \textbf{(2.73)}$$

Substituting (2.69.b) and (2.73) in (2.72.a, b)

$$\hat{J}_2^1 = J_2 + G\sqrt{\delta_1}\left(1-\frac{\delta_1}{3R}\right) \qquad \textbf{(2.74.a)}$$

$$\hat{J}_2^2 = J_2 + G\sqrt{\delta_2}\left(1-\frac{\delta_2}{3R}\right) \qquad \textbf{(2.74.b)}$$

Subtracting (2.74.a) from (2.74.b) one can obtain,

$$G = \frac{\hat{J}_2^1 - \hat{J}_2^2}{\sqrt{\delta_1}\left(1-\frac{\delta_1}{3R}\right) - \sqrt{\delta_2}\left(1-\frac{\delta_2}{3R}\right)} \qquad \textbf{(2.75)}$$

Substituting (2.75) in (2.74.a)

$$\hat{J}_2^1 = J_2 + \frac{\hat{J}_2^1 - \hat{J}_2^2}{\sqrt{\delta_1}\left(1-\frac{\delta_1}{3R}\right)-\sqrt{\delta_2}\left(1-\frac{\delta_2}{3R}\right)}\sqrt{\delta_1}\left(1-\frac{\delta_1}{3R}\right) \tag{2.76}$$

Organizing the terms,

$$J_2 = \frac{\sqrt{\delta_1}\left(1-\frac{\delta_1}{3R}\right)\hat{J}_2^2 - \sqrt{\delta_2}\left(1-\frac{\delta_2}{3R}\right)\hat{J}_2^1}{\sqrt{\delta_1}\left(1-\frac{\delta_1}{3R}\right)-\sqrt{\delta_2}\left(1-\frac{\delta_2}{3R}\right)} \tag{2.77}$$

At this stage, the terms of J_k - integral, namely J_1 and J_2 are numerically known. Therefore, the values of stress intensity factors can be determined.

Re-organizing (2.69.b)

$$K_{II} = -\frac{E' J_2}{2K_I} \tag{2.78}$$

Substituting (2.78) into (2.69.a)

$$J_1 = \frac{K_I^2 + \left(\frac{E' J_2}{2K_I}\right)^2}{E'} \tag{2.79}$$

Organizing the terms, the following equation is obtained,

$$K_I^4 - E' J_1 K_I^2 + \frac{1}{4}(E')^2 (J_2)^2 = 0 \tag{2.80.a}$$

The same equation can be obtained for K_{II} as follows

$$K_{II}^4 - E' J_1 K_{II}^2 + \frac{1}{4}(E')^2 (J_2)^2 = 0 \tag{2.80.b}$$

The four roots of this equation are as follows

$$R_1 = \left\{ \frac{E'}{2} \left(J_1 + \sqrt{(J_1)^2 + (J_2)^2} \right) \right\}^{1/2}$$

$$R_2 = -\left\{ \frac{E'}{2} \left(J_1 + \sqrt{(J_1)^2 + (J_2)^2} \right) \right\}^{1/2}$$

$$R_3 = \left\{ \frac{E'}{2} \left(J_1 - \sqrt{(J_1)^2 + (J_2)^2} \right) \right\}^{1/2}$$

$$R_4 = -\left\{ \frac{E'}{2} \left(J_1 - \sqrt{(J_1)^2 + (J_2)^2} \right) \right\}^{1/2} \qquad \textbf{(2.81.a-d)}$$

One of the four roots is Mode I stress intensity factor, K_I and another one is Mode II stress intensity factor, K_{II}.

The signs of the stress intensity factors are determined by monitoring relative normal and tangential displacements near the crack tip which are defined as

$$\Delta_n = u_2^+ - u_2^-$$

$$\Delta_t = u_1^+ - u_1^- \qquad \textbf{(2.82.a-b)}$$

where the superscripts + and − refer to the upper and lower crack surfaces, respectively.

In the finite element analysis, Δ_n and Δ_t are calculated in the close vicinity of the crack tip. A positive Δ_n value implies that crack is open near the crack tip and K_I is positive. Similarly, K_{II} is positive if $\Delta_t > 0$.

The value of *T*-stress can be determined after the calculation of Mode II SIF and *G* parameter defined in (2.75)

$$T_s = -\frac{\sqrt{2\pi}\, E'}{8 K_{II}} G \qquad \textbf{(2.83)}$$

CHAPTER 3

PROBLEM DEFINITION

In this study, inclined crack problems in isotropic FGM's under steady-state thermal loading are considered. This chapter is dedicated to explain the geometry and thermal boundary conditions of the problem.

3.1 Inclined Embedded Crack under Steady-State Thermal Loading

The geometry of an embedded inclined crack in a FGM layer is shown in Figure 3.1. The coordinate system is placed in the middle of the crack which has a length of $2a$. The thickness of the FGM layer is set to $h = h_1 + h_2$. The width of the FGM layer is W. The FGM layer has an embedded inclined crack at h_1 distance below the upper bound making an angle of ϕ with the positive x-axis. Geometrical parameters are taken as: $h_1/a = 2.0$, $h_2/a = 2.0$ and $W/a = 10.0$.

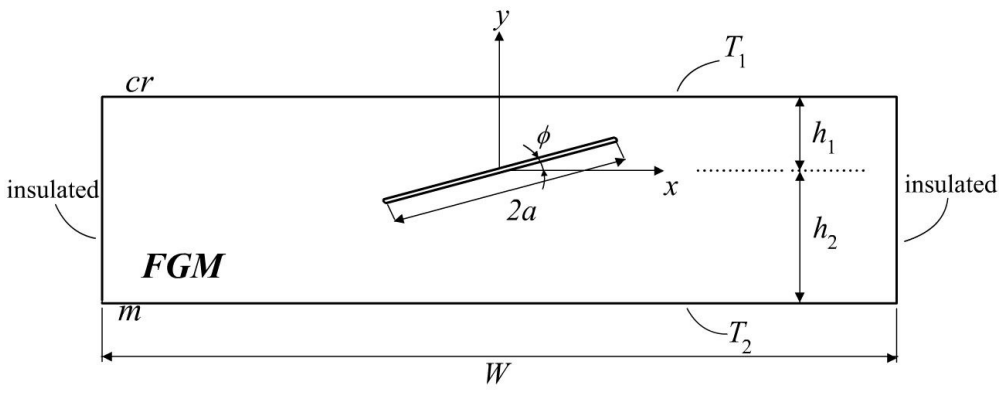

Figure 3.1 Geometry and boundary conditions of an inclined embedded crack under steady-state thermal loading

Initially, the specimen is at a reference temperature T_0 for which all stress components are assumed to be zero. Right and left end planes $x = \pm W/2$ are assumed to be insulated. Upper and lower bounds $y = h_1$, $y = -h_2$ are assumed to be kept at temperatures T_1 and T_2, respectively. Crack faces are assumed to be insulated.

Surfaces at $y = h_1$ and $y = -h_2$ are assumed to be 100% ZrO_2 and 100% Ni, respectively. Properties of ZrO_2 and Ni are given in Table 3.1 as follows:

Table 3.1 Thermomechanical Properties of ZrO_2 and Ni

	Modulus of Elasticity	*Poisson's Ratio*	*Thermal Expansion Coefficient*	*Thermal Conductivity*
Ni (*m*)	175.8 GPa	0.25	$13.91*10^{-6}$ °C^{-1}	7 W/mK
Zirconia (*cr*)	27.6 GPa	0.25	$10.01*10^{-6}$ °C^{-1}	1 W/mK

The graded thermomechanical properties of the FGM layer are varied only in y direction and represented in the following form

$$E(y) = E_{cr} + (E_m - E_{cr})\left(\frac{h_1 - y}{h_1 + h_2}\right)^{\gamma_1}, \qquad -h_2 < y < h_1,$$

$$\nu(y) = \nu_{cr} + (\nu_m - \nu_{cr})\left(\frac{h_1 - y}{h_1 + h_2}\right)^{\gamma_2}, \qquad -h_2 < y < h_1,$$

$$\alpha(y) = \alpha_{cr} + (\alpha_m - \alpha_{cr})\left(\frac{h_1 - y}{h_1 + h_2}\right)^{\gamma_3}, \qquad -h_2 < y < h_1,$$

$$k(y) = k_{cr} + (k_m - k_{cr})\left(\frac{h_1 - y}{h_1 + h_2}\right)^{\gamma_4}, \qquad -h_2 < y < h_1, \qquad \textbf{(3.1.a-d)}$$

where E is the modulus of elasticity

ν is Poisson's ratio

α is the thermal expansion coefficient

k is the thermal conductivity

Subscripts *cr* and *m* refer to 100% ceramic and metal surfaces, respectively. The FGM layer shown above is assumed to be in a deformation state of plane strain.

CHAPTER 4

FINITE ELEMENT IMPLEMENTATION

4.1 Finite Element Method

Finite element method is a numerical method that applies to real-world problems involving complicated physics, geometry, and/or boundary conditions. In this method, a given domain is divided into sub-domains, called *finite elements*, and an approximate solution to the problem is developed over each element. The main reason behind seeking approximate solution on a collection of finite elements is the fact that it is easier to represent a complicated function as a collection of simple polynomials. Subdivision of a whole domain and approximation approach allows accurate representation of complex geometries and inclusion of dissimilar material properties, just like FGMs. The finite element method converts a continuum problem to a discrete one, which is, converting a system with an infinite number of degrees of freedom into one with a finite number of degrees of freedom.

Finite element method of a system ultimately represents a set of algebraic equations among the values of the dependent variables of the system at the selected nodes of the domain. The coefficients of algebraic equations are typically integrals of approximation functions multiplied by the data of the problem. The exact solution of these integrals is not always possible due to algebraic complexity of the data. In such cases, it is natural to seek for numerical evaluation of these integral expressions.

Numerical integration involves approximation of the integrand by a polynomial of sufficient degree, since the integral of a polynomial can be evaluated exactly.
For instance, consider the integral;

$$I = \int_{x_a}^{x_b} F(x)\, dx \qquad \textbf{(4.1)}$$

The integrand $F(x)$ can be approximated by a polynomial such as,

$$F(x) \approx \sum_{i=1}^{N} F_i\, \psi_i(x) \qquad \textbf{(4.2)}$$

where F_i denotes the value of $F(x)$ at the i^{th} point

$\psi_i(x)$ denotes the polynomials of degree N-1

This representation can also be viewed as the finite element interpolation of $F(x)$.

The transformation of the geometry and variable coefficients of the governing equation, in this study being the J_k-integral, from the global coordinates (x, y) to natural coordinates (ξ, η) results in algebraically complex expressions and they preclude analytical evaluation of the integrals. The transformation of a given integral expression defined over master element to one on the domain Ω facilitates the numerical integration.

The numerical integration scheme that is used in this study is the Gauss-Legendre Quadrature. This integration method requires the integral to be evaluated on a specific domain with respect to a specific coordinate system, that is, the integral must be expressed over a square region $\hat{\Omega}$, with a natural coordinate system (ξ, η) to be such that $-1 \le (\xi, \eta) \le 1$. Therefore, some transformations must be made over the elements to utilize this integration scheme.

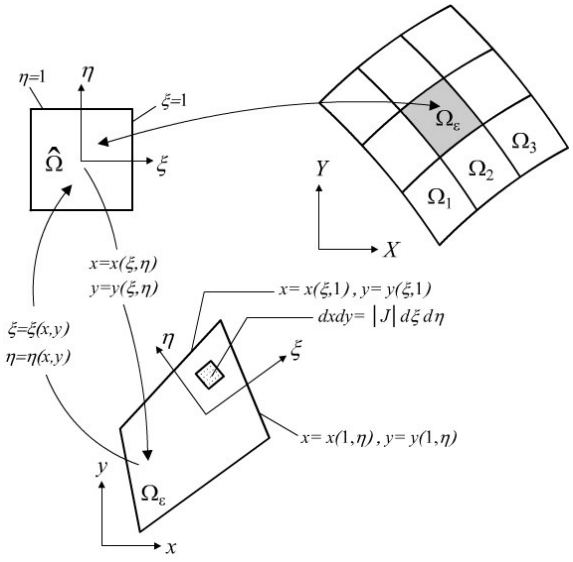

Figure 4.1 Mapping of a master rectangular element to an arbitrary quadrilateral element of a finite element mesh

Mapping of a rectangular element to a quadrilateral one is explained in Figure 4.1. It can be observed from Figure 4.1 that the natural coordinates and global coordinates are transformed such that the orientation of the element with respect to the global coordinates is also reflected to the transformation. The transformation relation between global coordinates and natural coordinates can be written as;

$$x(\xi,\eta)=\sum_{i=1}^{N}\psi_i(\xi,\eta)\,x_i$$

$$y(\xi,\eta)=\sum_{i=1}^{N}\psi_i(\xi,\eta)\,y_i \qquad \textbf{(4.3)}$$

where, $\psi_i(\xi,\eta)$ are the shape functions that are used to express the geometry or shape of the element.

The Gauss-Legendre Quadrature is based on the idea that the base Gauss points, x_i, and the Gauss weights W_i can be chosen so that the sum of the r+1 appropriately weighted values of the function yields the integral exactly when $F(x)$ is a polynomial of degree 2r+1.

A domain integral of the form,

$$I = \iint_{\Omega} F(x, y)\, dx\, dy \tag{4.4}$$

can be represented with Gauss-Legendre Quadrature as follows,

$$I = \int_{-1}^{1}\int_{-1}^{1} F(\xi,\eta)\,|J|\, d\xi\, d\eta = \int_{-1}^{1}\left[\sum_{i=1}^{r} F(\xi_i,\eta) W_i\right] d\eta = \sum_{j=1}^{r}\sum_{i=1}^{r} F(\xi_i,\eta_j) W_i W_j \tag{4.5}$$

where $|J|$ is the Jacobian of the element

A line integral of the form,

$$L = \int_{a}^{b} G(x) dx \tag{4.6}$$

can be represented with Gauss-Legendre Quadrature as follows,

$$L = \int_{-1}^{1} G(\xi) d\xi = \sum_{i=1}^{r} G(\xi_i) W_i \tag{4.7}$$

For a double integral given in (4.4), the Gauss point locations (Figure 4.2.b) and Gauss weights for the 2nd order Gauss-Legendre Quadrature are given as; [15]

$$(\xi_i\ ,\eta_j) = \left(\pm\ 1/\sqrt{3}\ ,\pm\ 1/\sqrt{3}\right)$$

$$W_i = W_j = 1 \tag{4.8}$$

It should be noted that the integrand of the numerical integration in (4.4) must be expressed in terms of natural coordinates (ξ, η). Therefore, for this study, the domain integral component of J_k-integral must be calculated at each of the four Gauss points.

For a line integral along x_1-axis given in (4.6) the Gauss point locations (Figure 4.3) and Gauss Weights for the 2nd order Gauss-Legendre Quadrature are given as; [15]

$$(\xi_i\ ,\eta_j) = \left(\pm\ 1/\sqrt{3}\ ,-1\right) \tag{4.9}$$

$$W_i = 1$$

Similar to the domain integral, the integrand of the numerical integration in (4.6) must be expressed in terms of natural coordinates (ξ, η). The integrands of line integral component of J_k-integral must be calculated at both of the Gauss points.

In this study ANSYS finite element program is used to calculate the mixed-mode SIFs under thermal loads. Problems involving thermomechanical conditions require a two-step analysis that is thermal analysis combined with structural analysis. First the thermal problem is solved, and nodal temperatures are stored in the database and then the structural analysis is run to determine the deformations and stresses induced on the model. Therefore, different element types are required for thermal and structural analysis. PLANE77 is used for thermal analysis and PLANE82 is utilized for the structural analysis. The same mesh is used for both of the analyses. The shape functions and node numbers are the same for both of the elements. The only difference between the two element types is that PLANE77 is a thermal element and can only store thermal degree of freedoms and properties for the element, such as temperature. However, PLANE82 is a structural element that can store displacement, stress and other structural values of the element. Both of the element types utilize 2nd order Gauss-Legendre Quadrature ($r = 2$), that is 2X2 Gauss points are used for integration and approximation processes. They are 8-noded quadrilaterals as it can be seen in Figure 4.2.a-b.

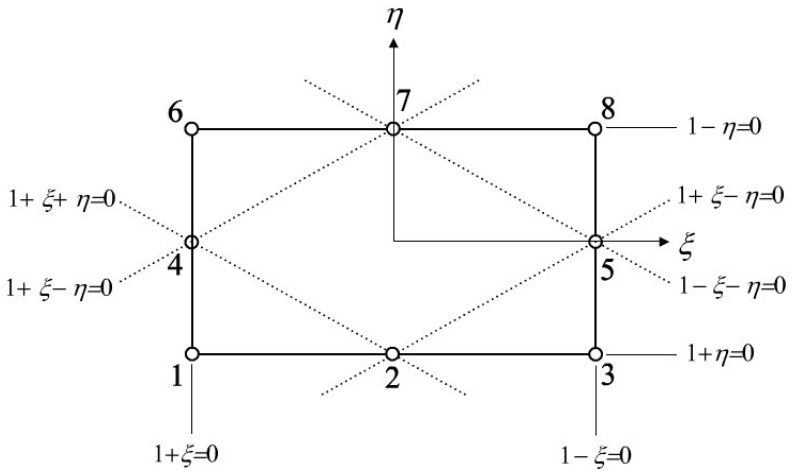

Figure 4.2.a Node numbers associated with PLANE82 structural element and PLANE77 thermal element.

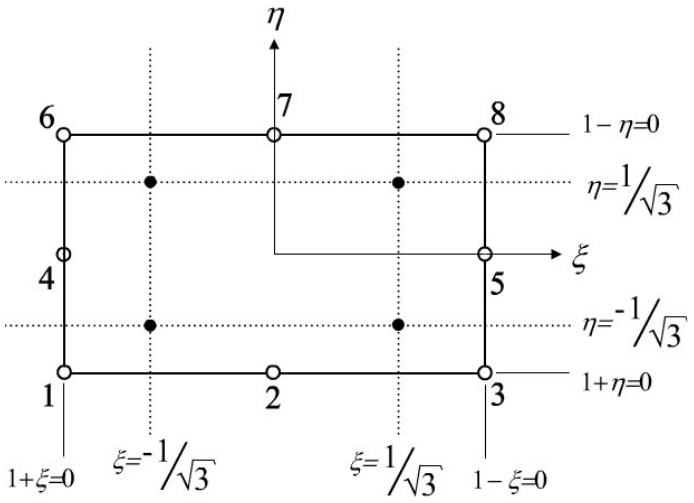

Figure 4.2.b Gauss point locations for domain integrals on 8-noded quadrilateral

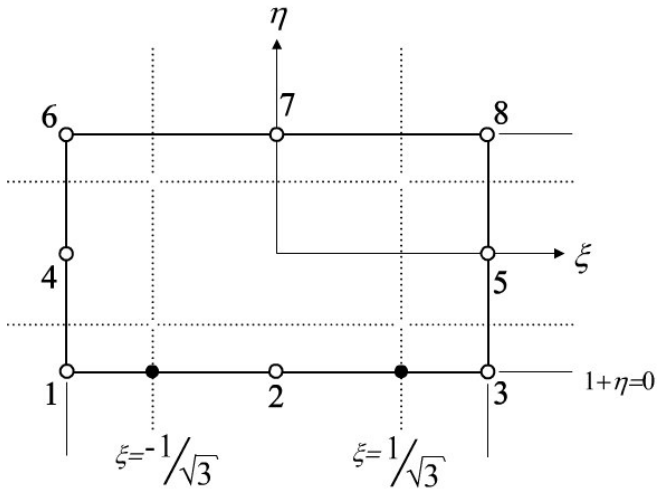

Figure 4.3 Gauss point locations for line integral along x-axis on 8-noded quadrilaterals

Shape functions for PLANE77 and PLANE82 elements are given as follows,

$$\psi_1 = -\frac{1}{4}(1-\xi)(1-\eta)(1+\xi+\eta) \qquad \psi_2 = \frac{1}{2}(1-\xi^2)(1-\eta)$$

$$\psi_3 = -\frac{1}{4}(1+\xi)(1-\eta)(1-\xi+\eta) \qquad \psi_4 = \frac{1}{2}(1-\xi)(1-\eta^2) \qquad \textbf{(4.10.a-h)}$$

$$\psi_5 = \frac{1}{2}(1+\xi)(1-\eta^2) \qquad \psi_6 = -\frac{1}{4}(1-\xi)(1+\eta)(1+\xi-\eta)$$

$$\psi_7 = \frac{1}{2}(1-\xi^2)(1+\eta) \qquad \psi_8 = -\frac{1}{4}(1+\xi)(1+\eta)(1-\xi-\eta)$$

Equation (4.3) expresses the global coordinate transformation to the natural coordinates. Consider a dependent variable such as the displacement of the element nodes in global *x* direction, *u*. The finite element method allows the users to create two different meshes of elements for the approximation of the geometry, being global coordinate *x*, and the interpolation of dependent variable, being the displacement *u*.

Depending on the degree of geometry approximation and the degree of dependent variable interpolation, finite element formulations are classified into three categories:

- Subparametric Formulation represents the geometry with lower order elements than those used to interpolate for the dependent variable.

- Isoparametric Formulation utilizes the same element to approximate the geometry and interpolate the dependent variable.

- Superparametric Formulation utilizes higher order elements to represent the geometry.

In this study, isoparametric formulation will be used to investigate the behavior of functionally graded materials under mixed-mode conditions. That is, the same elements, therefore the same shape functions, will be utilized to approximate the geometry and interpolate the dependent unknowns.

$$x(\xi,\eta)=\sum_{i=1}^{N}\psi_i(\xi,\eta)\,x_i \qquad \text{Transformation of global coordinate } x \qquad \textbf{(4.11.a-d)}$$

$$y(\xi,\eta)=\sum_{i=1}^{N}\psi_i(\xi,\eta)\,y_i \qquad \text{Transformation of global coordinate } y$$

$$u(\xi,\eta)=\sum_{i=1}^{N}\psi_i(\xi,\eta)\,u_i \qquad \text{Transformation of displacement in } x \text{ direction, } u$$

$$v(\xi,\eta)=\sum_{i=1}^{N}\psi_i(\xi,\eta)\,v_i \qquad \text{Transformation of displacement in } y \text{ direction, } v$$

4.2 Finite Element Solution Procedure

In this study, a finite element method procedure is developed for the calculation of J_k-integral. For this purpose, a computer code is developed in ANSYS [11] by utilizing Ansys Parametric Design Language. The code simply aims at the evaluation of stress intensity factors around the crack tip in a functionally graded medium under thermal loads. As mentioned earlier by (2.69), SIF's are related to the components of J_k-integral, namely J_1 and J_2. In this chapter, the numerical evaluation of J_1 and $\hat{J}_2$ which are derived in (2.48) and (2.70) respectively are explained in detail.

The analytical evaluation of J_1-integral in FGM layer is given by (2.48).

Re-organizing this equation,

$$J_1 = \iint_{\Omega} \left(\sigma_{ij}\, u_{i,1}\, q_{,j} - W\, \delta_{1j}\, q_{,j} - \left(W_{,1}\right)_{\text{expl}} q \right) d\Omega \qquad \textbf{(4.12)}$$

Let

$$F_n(\xi,\eta) = \left(\sigma_{ij}\, u_{i,1}\, q_{,j} - W\, \delta_{1j}\, q_{,j} - \left(W_{,1}\right)_{\text{expl}} q \right) |J|_n \qquad \textbf{(4.13)}$$

where $|J|_n$ is the Jacobian of the nth element

then for the nth element,

$$J_{1n} = \int_{-1}^{1} \int_{-1}^{1} F_n(\xi,\eta)\, d\xi\, d\eta \qquad \textbf{(4.14)}$$

Applying the Gauss-Legendre Quadrature given in (4.5) and substituting the weight values given in (4.8), the following is obtained

$$J_{1n} = \sum_{j=1}^{2} \sum_{i=1}^{2} F_n\left(\xi_i, \eta_j\right) \qquad \textbf{(4.15)}$$

Summing J_{1n} contributions from all elements, J_1 can be calculated.

Considering (4.15) together with (4.8), it can be concluded that in order to evaluate J_1 integral with Gauss-Legendre Quadrature, the integrand $F(\xi,\eta)$must be evaluated at all Gauss points. Therefore, the values of σ_{ij}, $u_{i,1}$, W, $q_{,j}$, $(W_{,1})_{\text{expl}}$ and q at four Gauss points of an element must be determined to evaluate the integral.

Considering the second component of J_k-integral, namely J_2-integral, it is concluded before in (2.70) that $\hat{J}_2$ must be calculated in order to evaluate J_2-integral.

Reorganizing (2.70)

$$\hat{J}_2 = \underbrace{\iint_{\Omega}\left(\sigma_{ij}\,u_{i,2}\,q_{,j} - W\,\delta_{2j}\,q_{,j} - (W_{,2})_{\text{expl}}\,q\right)d\Omega}_{\text{Domain Integral Part}} \underbrace{-\int_{0}^{R-\delta}\left(W^{+}-W^{-}\right)\frac{x}{R}dx}_{\text{Line Integral Part}} \qquad \textbf{(4.16)}$$

When the domain integral part is considered, some similarities are realized between J_1-integral and this part. It can be observed that, the values of $u_{i,2}$, $(W_{,2})_{\text{expl}}$ at the Gauss points are additionally required for the evaluation of this part.

To sum up, the values of the variables in Table 4.1 must be known at every four Gauss points of an element, in order to evaluate the domain integrals over that element.

Table 4.1 The variables of J_1 and $\hat{J}_2$ integrands that must be evaluated at every Gauss point.

Indicial	*Explanation*	*Explicit*	*Needed for*
σ_{ij}	Stress tensor	$\sigma_{11}, \sigma_{22}, \sigma_{12}$	Both
$u_{i,1}$	Derivative of displacements with respect to x_1-axis	$\frac{\partial u_1}{\partial x}$, $\frac{\partial u_2}{\partial x}$	J_1
$u_{i,2}$	Derivative of displacements with respect to x_2-axis	$\frac{\partial u_1}{\partial y}$, $\frac{\partial u_2}{\partial y}$	$\hat{J}_2$
W	Mechanical Strain energy density function	(2.51)	Both
$(W_{,1})_{\text{expl}}$	Derivative of W with respect to x-axis	(2.52)	J_1
$(W_{,2})_{\text{expl}}$	Derivative of W with respect to y-axis	(2.57)	$\hat{J}_2$
$\lvert J \rvert$	Jacobian of transformation	$\lvert J \rvert = \frac{\partial x}{\partial \xi}\frac{\partial y}{\partial \eta} - \frac{\partial y}{\partial \xi}\frac{\partial x}{\partial \eta}$	Both
q	q-function	(C.1)	Both
$q_{,j}$	Derivative of q-function	(C.2) and (C.3)	Both

The evaluation of J_2 integral additionally requires the determination of the following line integral, the value of which is also calculated by Gauss- Legendre Quadrature.

$$L = \int_0^{R-\delta} \left(W^+ - W^-\right)\frac{x}{R}dx \qquad \textbf{(4.17)}$$

The locations *(x, y)* and the displacements *(u, v)* of Gauss points can be calculated numerically with the use of isoparametric formulations given in (4.11.a-d). However, in order to evaluate the Jacobian of transformation, the values of $\frac{\partial x}{\partial \xi}, \frac{\partial y}{\partial \eta}, \frac{\partial y}{\partial \xi}, \frac{\partial x}{\partial \eta}$ are must be known.

When (4.11.a) and (4.11.b) are differentiated with respect to ξ and η,

$$\frac{\partial x(\xi,\eta)}{\partial \xi} = \sum_{i=1}^{8} \frac{\partial \psi_i(\xi,\eta)}{\partial \xi} x_i$$

$$\frac{\partial x(\xi,\eta)}{\partial \eta} = \sum_{i=1}^{8} \frac{\partial \psi_i(\xi,\eta)}{\partial \eta} x_i$$

$$\frac{\partial y(\xi,\eta)}{\partial \xi} = \sum_{i=1}^{8} \frac{\partial \psi_i(\xi,\eta)}{\partial \xi} y_i$$

$$\frac{\partial y(\xi,\eta)}{\partial \eta} = \sum_{i=1}^{8} \frac{\partial \psi_i(\xi,\eta)}{\partial \eta} y_i \qquad \textbf{(4.18.a-d)}$$

where, $\frac{\partial \psi_i(\xi,\eta)}{\partial \xi}$ and $\frac{\partial \psi_i(\xi,\eta)}{\partial \eta}$ are the derivatives of shape functions and can be evaluated by differentiating (4.10.a-h) with respect to ξ and η,

x_i and y_i are the locations of 8-nodes of the element.

As reported in Table 4.1, the values of $\frac{\partial u}{\partial x}$, $\frac{\partial v}{\partial x}$, $\frac{\partial u}{\partial y}$, $\frac{\partial v}{\partial y}$ are also required for the evaluation. When (4.11.c) and (4.11.d) are differentiated with respect to x and y,

$$\frac{\partial u}{\partial x} = \sum_{i=1}^{8} \frac{\partial \psi_i(x,y)}{\partial x} u_i$$

$$\frac{\partial u}{\partial y} = \sum_{i=1}^{8} \frac{\partial \psi_i(x,y)}{\partial y} u_i$$

$$\frac{\partial v}{\partial x} = \sum_{i=1}^{8} \frac{\partial \psi_i(x,y)}{\partial x} v_i$$

$$\frac{\partial v}{\partial y} = \sum_{i=1}^{8} \frac{\partial \psi_i(x,y)}{\partial y} v_i \qquad \textbf{(4.19.a-d)}$$

where, $\frac{\partial \psi_i(x,y)}{\partial x}$ and $\frac{\partial \psi_i(x,y)}{\partial y}$ are the derivatives of shape functions given by (4.10.a-h) and can be evaluated by firstly transforming and substituting (4.11.a) and (4.11.b) and then differentiating (4.10.a-h) with respect to x and y.

u_i and v_i are the 8-nodal displacements of the element.

When the total strain definition in (2.4.a-f) is utilized, the total engineering strains can be evaluated easily at the Gauss points of the element.

Substituting (4.19.a-d) into (2.4.a-f) the total strains for plane strain case are calculated as follows

$$\varepsilon_x = \sum_{i=1}^{8} \frac{\partial \psi_i(x,y)}{\partial x} u_i$$

$$\varepsilon_y = \sum_{i=1}^{8} \frac{\partial \psi_i(x,y)}{\partial y} v_i$$

$$\gamma_{xy} = \sum_{i=1}^{8} \frac{\partial \psi_i(x,y)}{\partial y} u_i + \sum_{i=1}^{8} \frac{\partial \psi_i(x,y)}{\partial x} v_i \qquad \textbf{(4.20.a-c)}$$

Once the total strains are known, the stresses at the Gauss points can be calculated with the use of (2.9) which gives the relation between stresses and strains under thermal loads.

Mechanical strain energy density function, *W*, is expresses in terms of total strain components by (2.51). Therefore, *W* is a known quantity, once the total strains are known. However, the explicit derivatives of the mechanical strain energy density function $\left(W_{,1}\right)_{\text{expl}}$ and $\left(W_{,2}\right)_{\text{expl}}$ which are given by (2.52) and (2.57) respectively are not calculated directly. The evaluation of these variables requires the derivatives of Lame's constants and temperature difference parameter with respect to a given Cartesian coordinate system x and y these derivatives are $\frac{\partial \mu}{\partial x}, \frac{\partial \lambda}{\partial x}, \frac{\partial \beta}{\partial x}, \frac{\partial \alpha}{\partial x}, \frac{\partial \theta}{\partial x}, \frac{\partial \mu}{\partial y}, \frac{\partial \lambda}{\partial y}, \frac{\partial \beta}{\partial y}, \frac{\partial \alpha}{\partial y}, \frac{\partial \theta}{\partial y}$.

By employing the preceding isoparametric formulation the derivatives with respect to x can be calculated as follows;

$$\frac{\partial \mu}{\partial x} = \sum_{i=1}^{8} \frac{\partial \psi_i}{\partial x} \mu_i$$

$$\frac{\partial \lambda}{\partial x} = \sum_{i=1}^{8} \frac{\partial \psi_i}{\partial x} \lambda_i$$

$$\frac{\partial \beta}{\partial x} = \sum_{i=1}^{8} \frac{\partial \psi_i}{\partial x} \beta_i$$

$$\frac{\partial \alpha}{\partial x} = \sum_{i=1}^{8} \frac{\partial \psi_i}{\partial x} \alpha_i$$

$$\frac{\partial \theta}{\partial x} = \sum_{i=1}^{8} \frac{\partial \psi_i}{\partial x} \theta_i \qquad \textbf{(4.21.a-e)}$$

Similarly, derivatives with respect to global coordinate y are as follows;

$$\frac{\partial \mu}{\partial y} = \sum_{i=1}^{8} \frac{\partial \psi_i}{\partial y} \mu_i$$

$$\frac{\partial \lambda}{\partial y} = \sum_{i=1}^{8} \frac{\partial \psi_i}{\partial y} \lambda_i$$

$$\frac{\partial \beta}{\partial y} = \sum_{i=1}^{8} \frac{\partial \psi_i}{\partial y} \beta_i$$

$$\frac{\partial \alpha}{\partial y} = \sum_{i=1}^{8} \frac{\partial \psi_i}{\partial y} \alpha_i$$

$$\frac{\partial \theta}{\partial y} = \sum_{i=1}^{8} \frac{\partial \psi_i}{\partial y} \theta_i \qquad \textbf{(4.22.a-e)}$$

where, $\mu_i, \lambda_i, \beta_i$ are Lame's constants at 8-nodes of the element

α_i is the thermal expansion coefficient at 8-nodes of the element

θ_i is the temperature difference at 8-nodes of the element

Up to this point, the calculation of J_1 and $\hat{J}_2$-integrals are considered. Once these two terms are known, mixed-mode stress intensity factors calculation is straightforward as explained in Section 2.3.

The relation between J_2 and $\hat{J}_2$ given by (2.77) is employed to find out J_2-integral value. Mode I stress intensity factor, K_I and Mode II stress intensity factor K_{II} can be evaluated by simply finding the roots of (2.80.a) and (2.80.b), respectively.

CHAPTER 5

RESULTS AND DISCUSSION

5.1 Thermal SIF's for an edge crack in an FGM Layer: Comparisons

In order to validate the equivalent domain integral approach, the calculation of Mode I SIF's for a horizontal edge crack in an FGM layer shown in Figure 5.1 is considered.

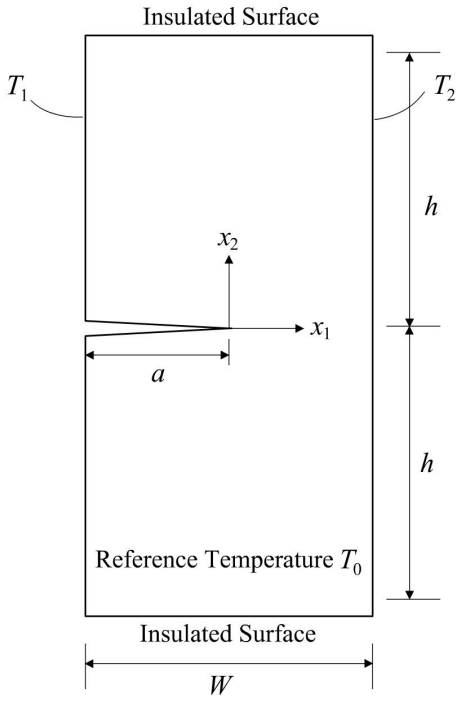

Figure 5.1 A functionally graded layer under steady-state thermal loading

The FGM layer of width W contains an edge crack length of which is denoted by a. The half-height is taken as $h = 4 * W$. Initially, the layer is assumed to be

kept at a uniform reference temperature of T_0. Subsequently, the temperatures of surfaces at $x_1 = 0$ and $x_1 = W$ are decreased to $T_1 = 0.2T_0$ and $T_1 = 0.5T_0$, respectively. All other surfaces including the crack faces are assumed to be insulated.

The material behavior of the FGM layer is isotropic and in accordance with Figure 5.1, the material property distributions can be presented as follows,

$$\begin{aligned} E(x_1) &= E_0 \exp[\beta(x_1 + a)] \\ \alpha(x_1) &= \alpha_0 \exp[\varpi(x_1 + a)] \\ k(x_1) &= k_0 \exp[\delta(x_1 + a)] \\ \upsilon &= 0.3 \end{aligned} \qquad \textbf{(5.1.a,c)}$$

where, β, ϖ and δ are the nonhomogeneity constants for elastic modulus, thermal expansion coefficient and thermal conductivity, respectively.

The constants of E_0, α_0 and k_0 are given by,

$$E_0 = E(x_1 = -a)\ ,\ \alpha_0 = \alpha(x_1 = -a) \text{ and } k_0 = k(x_1 = -a) \qquad \textbf{(5.2.a-c)}$$

It can be noted that parameters other than the Poisson's ratio have exponential variations with respect to x_1 direction. However, the Poisson's ratio possesses a constant value of 0.3 throughout the FGM layer in order to make the problem analytically tractable in [13].

In order to authenticate the developed finite element method, some comparisons of the thermal stress intensity factors to those reported by Walters *et al.* [16] and Erdogan and Wu [17] are presented in Table 4.1. The results of Walters *et al.* [16] and Erdogan and Wu [17] are given by means of a newly introduced parameter, normalized stress intensity factor.

The normalized stress intensity factor is defined as,

$$K_{\text{In}} = \frac{K_I (1-\upsilon)}{E_0 \alpha_0 T_0 \sqrt{\pi a}} \tag{5.3}$$

Erdogan and Wu [17] examined this problem analytically utilizing Fourier Transform techniques and the method of singular integral equations. Walters *et al.* [16] analyzed the case using a three dimensional finite element model with a domain integral approach.

Table 5.1 Comparisons of the normalized Mode I stress intensity factor K_{In} for the case of plane strain condition, with crack ratio of a/W=0.5 and nonhomogeneity constants $\beta W = \ln(10)$, $\varpi W = \ln(10)$, $\delta W = \ln(10)$

	Domain sizes	$T_1 = 0.2T_0 \quad T_2 = 0.5T_0$
EDI	$R/a = 0.1$	0.0338
	$R/a = 0.2$	0.0340
	$R/a = 0.3$	0.0340
	$R/a = 0.4$	0.0340
Walters *et al.* [16]		0.0335
Dağ [13]		0.0339
Erdogan and Wu [17]		0.0335

Note that four different domain radii are used in EDI calculations, as seen in Figure 5.2. The results calculated for various domain sizes, $R/a = 0.1, 0.2, 0.3, 0.4$ are in good agreement with each other which implies that EDI possesses the required domain independence.

Examining the results given by Table 5.1, it can be observed that the normalized stress intensity factors obtained using EDI agree quite well with those given by Walters *et al.* [16] and Erdogan and Wu [17].

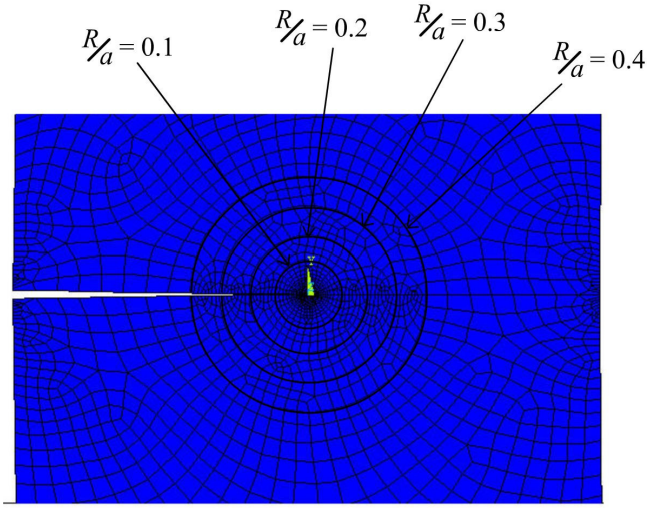

Figure 5.2 Circular domains around the crack tip, for the isotropic FGM layer shown in Figure 5.1 considering plane strain.

Identical finite element meshes are utilized in the solutions of different domain sizes. While conducting a thermo-structural analysis, the meshes are required to be finely tuned. Especially the mesh in the circular domain is refined in order to evaluate the stress intensity factors within a high degree of accuracy. For example, for the evaluation of the domain $R/a = 0.4$, the mesh in the domain possesses 30511 quadrilateral elements.

The deformed shape of the developed finite element model can be seen in Figure 5.3. The temperature distribution in the FGM layer is plotted in Figure 5.4. The stress distribution in the FGM layer can be seen in Figure 5.5.

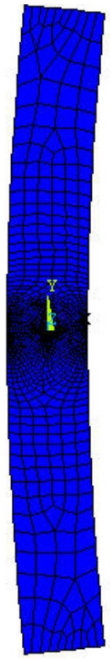

Figure 5.3 Deformed shape of the finite element model of the FGM layer $a/W = 0.5$, $\beta W = \ln(10)$, $\varpi W = \ln(10)$, $\delta W = \ln(10)$, $T_1 = 0.2 * T_0$, $T_2 = 0.5 * T_0$

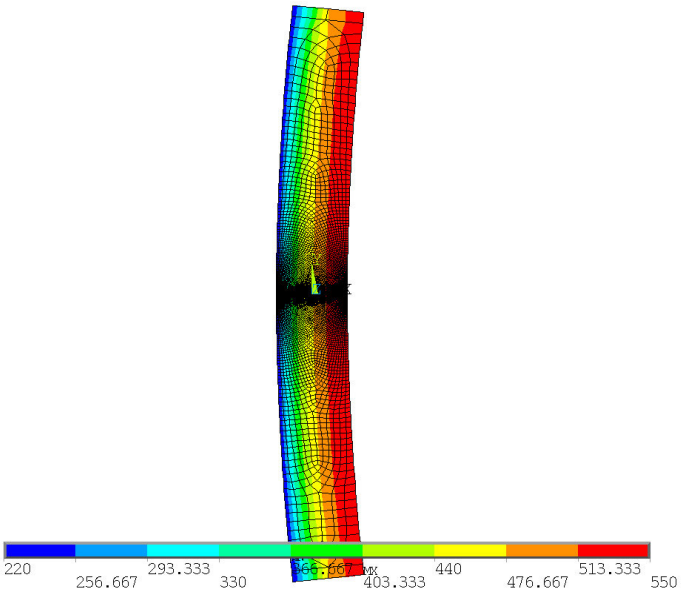

Figure 5.4 Temperature distribution in the FGM layer $a/W = 0.5$, $\beta W = \ln(10)$, $\varpi W = \ln(10)$, $\delta W = \ln(10)$, $T_1 = 0.2 * T_0$, $T_2 = 0.5 * T_0$

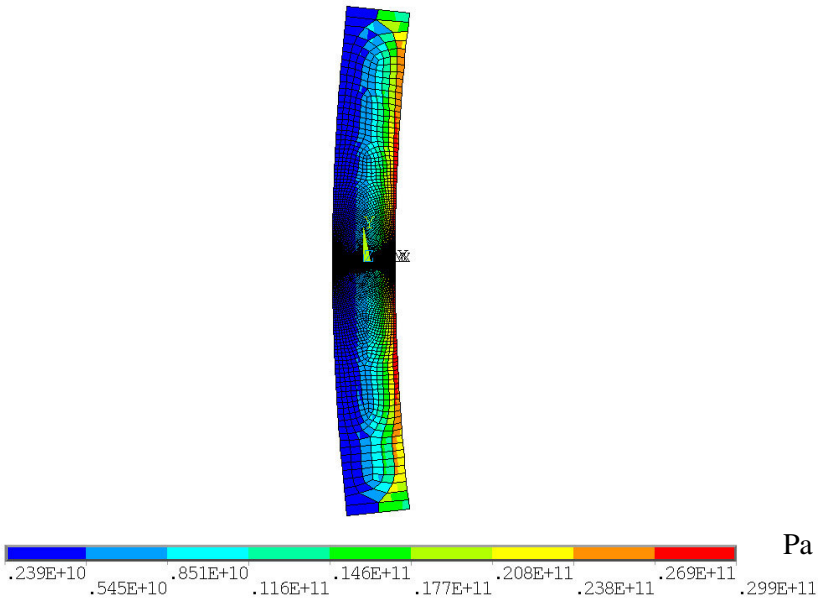

Figure 5.5 Principal stress distribution in the FGM layer $a/W = 0.5$, $\beta W = \ln(10)$, $\varpi W = \ln(10)$, $\delta W = \ln(10)$, $T_1 = 0.2 * T_0$, $T_2 = 0.5 * T_0$

5.2 An Inclined Embedded Crack in an FGM Layer under Steady-State Thermal Stresses

In this section sample results are given and discussed for the problem defined in Chapter 3. Thermal stress intensity factors are presented and compared to the ones obtained by a Displacement Correlation Technique [18]. Additionally, several result sets for thermal stress intensity factors and T-stress are plotted and discussed. Basically, the response of the inclined crack to variations in the orientation angle is examined. Additionally, the effect of changing thermal expansion coefficient and thermal conductivity on resulting parameters are analyzed.

5.2.1 Finite Element Results

The inclined embedded crack problem is redefined in detail in Figure 5.6. Upper crack tip and lower crack tips are named as A and B, respectively.

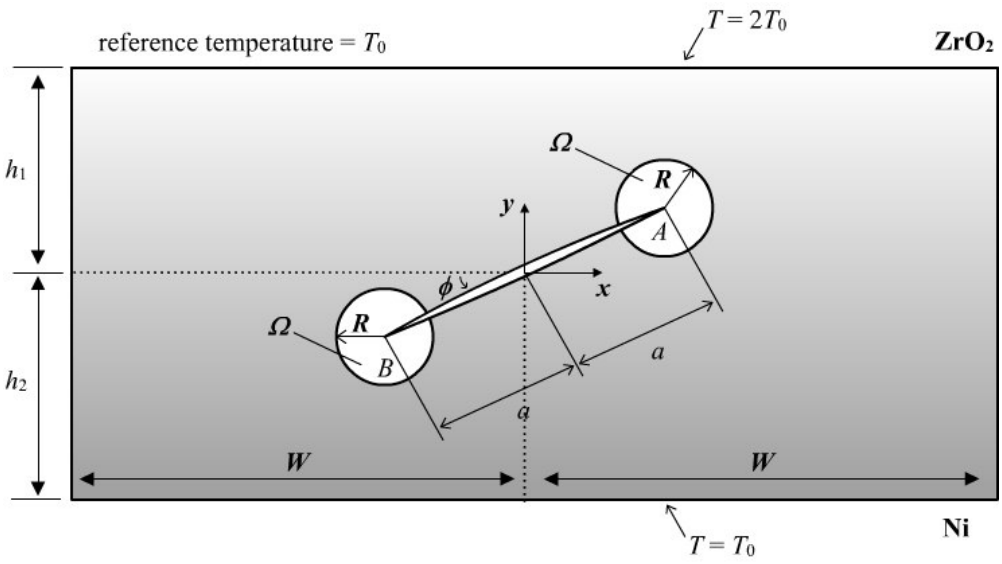

Figure 5.6 Details of the geometry and thermal loading conditions for the inclined crack problem

Graded medium is modeled with triangular shaped elements. A triangular-shaped element is formed by defining the same node number for node locations 6, 7 and 8 which are given in Figure 4.2.a. Material properties throughout the FGM layer change according to given functions by (3.1).

Whole finite element mesh for an orientation angle of $\phi = \pi/6$ is presented in Figure 5.7. Whole mesh contains 60488 triangular elements.

The bottom up modeling approach is followed during the modeling of the problem. While building the model from bottom up, the model is initially defined by utilizing the lowest-order solid model entities, keypoints. Keypoints are defined within the currently active Global Cartesian coordinate system. After initial pattern of keypoints are created, lines are defined by connecting these keypoints. Crack faces are modeled as two separate lines. Meshes are defined over areas, which are defined by enclosing boundaries, in this case being lines.

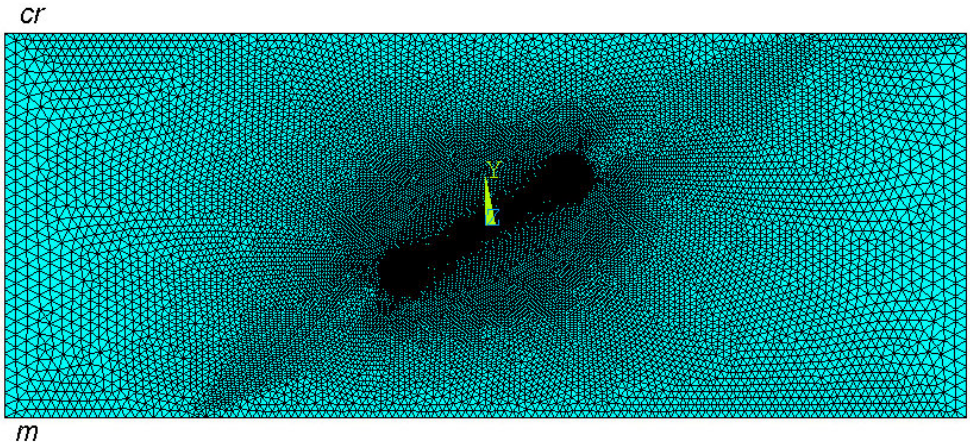

Figure 5.7 Finite element mesh for Inclined Embedded Crack under thermal loading with $a/W = 0.1$, $h_2/a = 2.0$, $h_1/a = 2.0$ and nonhomogeneity constants of $\gamma_1 = 1.5$, $\gamma_2 = 1.5$, $\gamma_3 = 0.5$, $\gamma_4 = 2.0$

Deformed shape of the whole finite element model is displayed in Figure 5.8. Deformed shapes of finite element meshes near crack tip A and crack tip B are presented in Figure 5.9 and 5.10, respectively. The domain of the both crack tips are modeled with 11722 elements for domain ratio of $R/a = 0.1$.

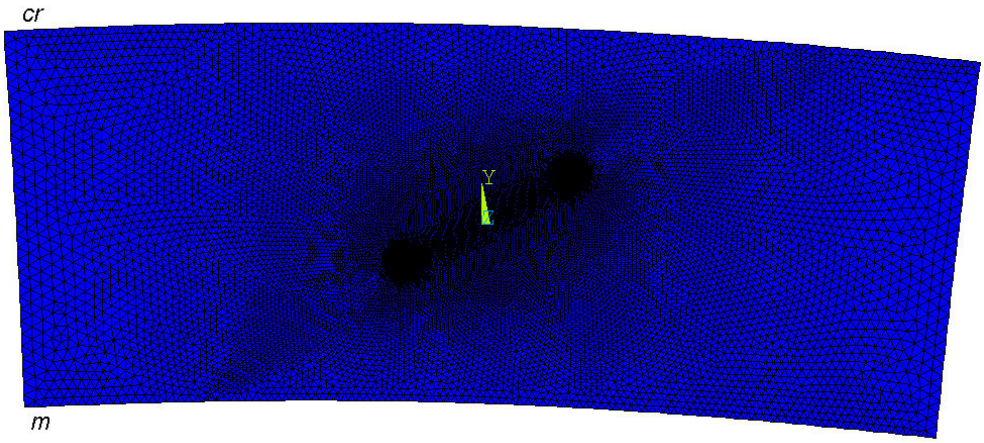

Figure 5.8 Deformed shape of finite element mesh of inclined embedded crack with $a/W = 0.1$, $h_2/a = 2.0$, $h_1/a = 2.0$ and nonhomogeneity constants of $\gamma_1 = 1.5$, $\gamma_2 = 1.5$, $\gamma_3 = 0.5$, $\gamma_4 = 2.0$

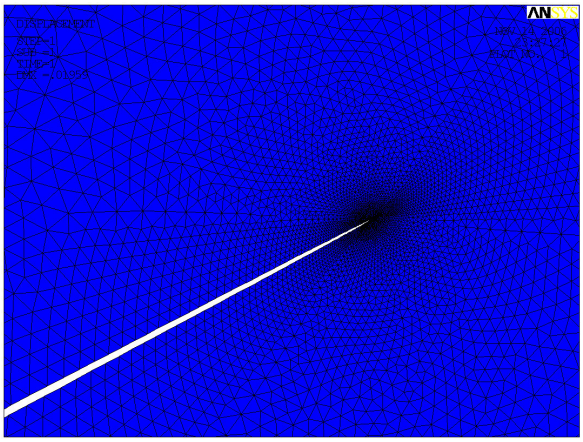

Figure 5.9 Deformed shape near the crack tip A with $a/W = 0.1$, $h_2/a = 2.0$, $h_1/a = 2.0$ and nonhomogeneity constants of $\gamma_1 = 1.5$, $\gamma_2 = 1.5$, $\gamma_3 = 0.5$, $\gamma_4 = 2.0$

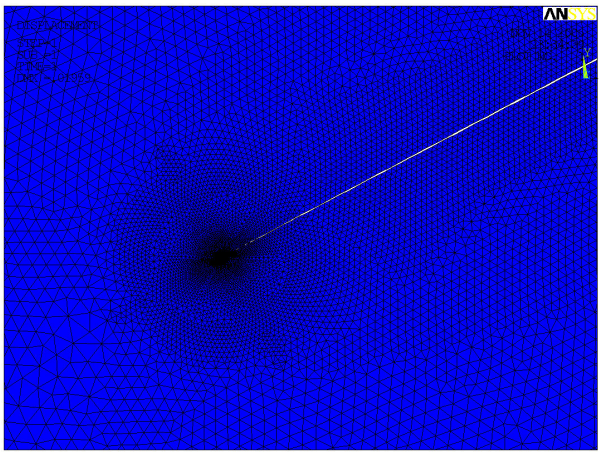

Figure 5.10 Deformed shape near the crack tip B with $a/W = 0.1$, $h_2/a = 2.0$, $h_1/a = 2.0$ and nonhomogeneity constants of $\gamma_1 = 1.5$, $\gamma_2 = 1.5$, $\gamma_3 = 0.5$, $\gamma_4 = 2.0$

The response of the finite element model to the thermal boundary conditions is viewed in Figure 5.11. Thermal constraints on upper and lower boundary layers are defined as $T_1 = 2 * T_0$ and $T_2 = T_0$, respectively.

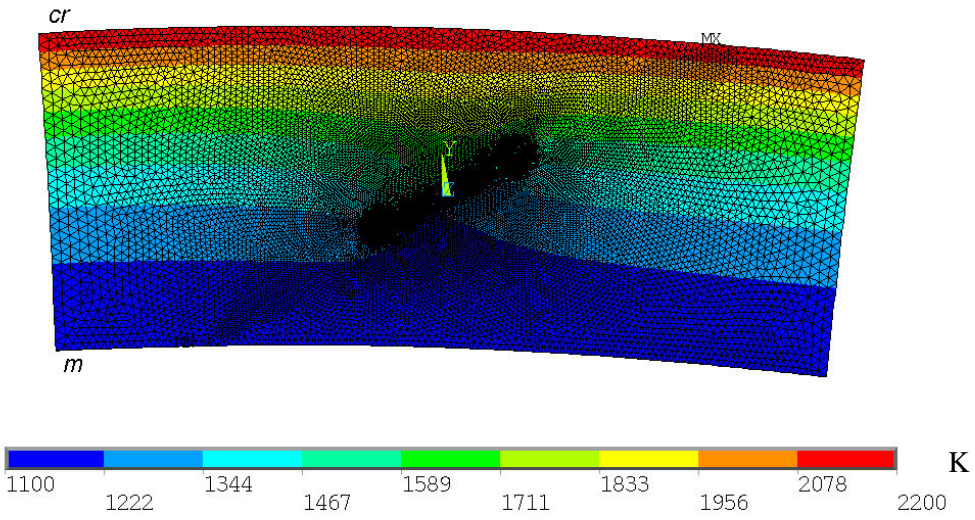

Figure 5.11 Temperature distribution of finite element mesh with $T_0 = 1100K$ and $a/W = 0.1$, $h_2/a = 2.0$, $h_1/a = 2.0$ and nonhomogeneity constants of $\gamma_1 = 1.5$, $\gamma_2 = 1.5$, $\gamma_3 = 0.5$, $\gamma_4 = 2.0$

Temperature distributions around crack tip A and crack tip B are presented in Figure 5.12 and Figure 5.13, respectively. Crack faces are modeled as insulated for simplicity. There is no heat conduction between crack faces and temperature distributions are distorted. Another approach of applying thermal boundary conditions to crack faces could be insulating the crack faces partially.

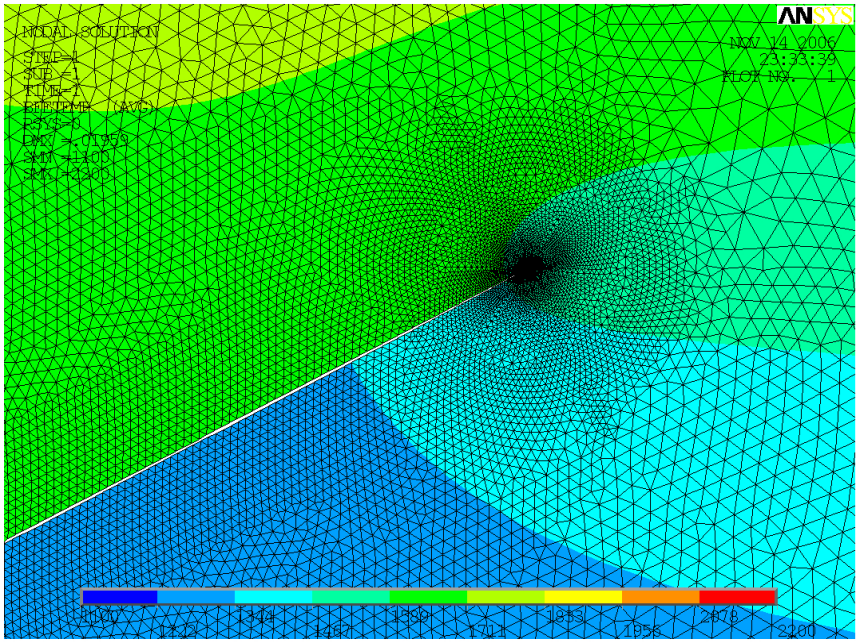

Figure 5.12 Temperature distribution around crack tip A with $T_0 = 1100K$ and $a/W = 0.1$, $h_2/a = 2.0$, $h_1/a = 2.0$ and nonhomogeneity constants of $\gamma_1 = 1.5$, $\gamma_2 = 1.5$, $\gamma_3 = 0.5$, $\gamma_4 = 2.0$

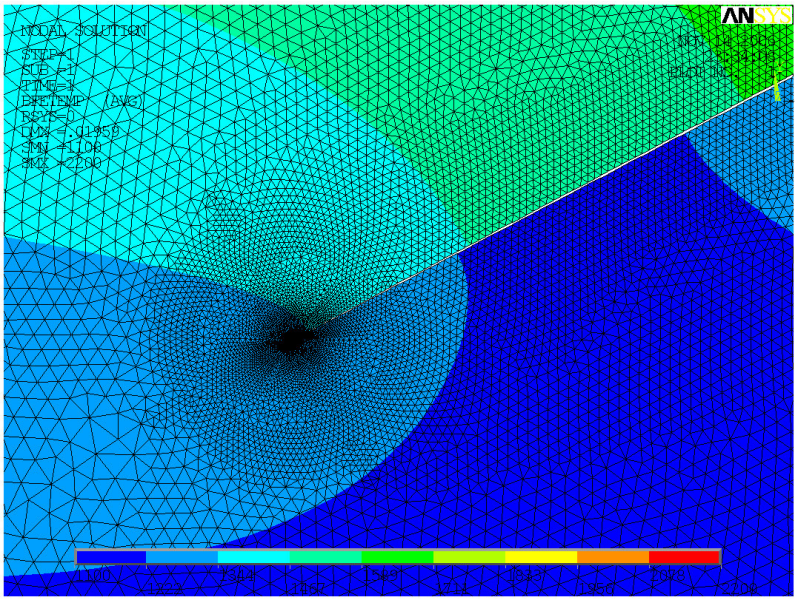

Figure 5.13 Temperature distribution around crack tip B with $T_0 = 1100K$ and $a/W = 0.1$, $h_2/a = 2.0$, $h_1/a = 2.0$ and nonhomogeneity constants of $\gamma_1 = 1.5$, $\gamma_2 = 1.5$, $\gamma_3 = 0.5$, $\gamma_4 = 2.0$

5.2.2 Domain Independence: Comparison to DCT

In order to investigate the effect of changing material properties and angle of crack on the behavior of parameters, the thermal stress intensity factors and T-stresses are normalized. Normalized thermal stress intensity factors are defined as follows,

$$K_{In} = \frac{K_I}{K_0} \qquad K_{IIn} = \frac{K_{II}}{K_0} \qquad \textbf{(5.3.a-b)}$$

where, $K_0 = \sigma_0 \sqrt{\pi a}$ and $\sigma_0 = E_{cr} \alpha_{cr} T_0$. **(5.4.a-b)**

Normalized T - stress is defined as

$$T_{sn} = \frac{T_s}{\sigma_0} \qquad \textbf{(5.5)}$$

The stress intensity factors for the layer shown in Figure 3.1 are calculated using both the Equivalent Domain Integral method and Displacement Correlation Technique in order to validate the accuracy of the EDI technique. DCT method simply matches the displacement values of crack faces with the asymptotic stress fields. The APDL source code for the DCT is developed in the thesis by Yılmaz [18].

Steady-state stress intensity factors for various values of γ_3 are computed and presented in Table 5.2. Four different domain sizes $R/a = 0.1$, 0.2, 0.3 and 0.4 are modeled and corresponding results for each of them are presented in Table 5.2. Figure 5.14 presents four domain radii which are utilized to prove the domain independence of J_k-integral.

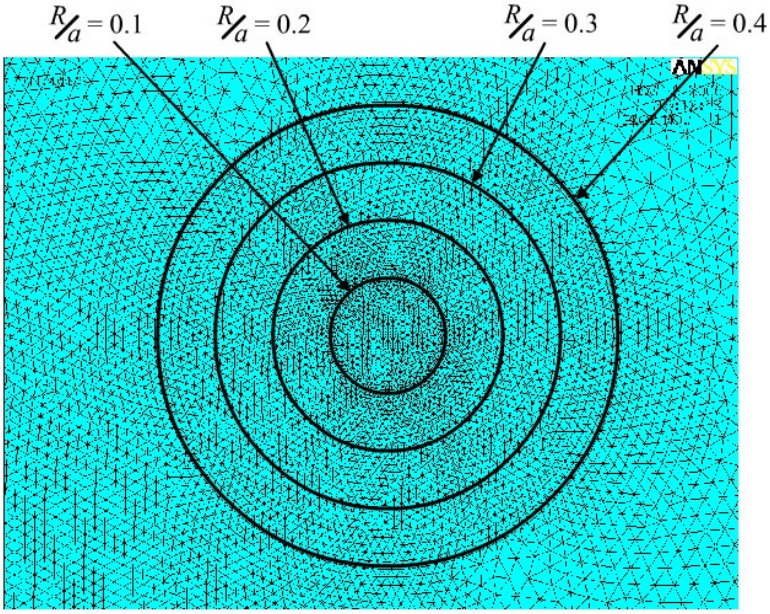

Figure 5.14 Finite element mesh of different domains $R/a = 0.1$, 0.2, 0.3 and 0.4

Two different values of γ_3 and four different values of ϕ are considered in the calculations. The comparisons of the normalized stress intensity factors calculated by EDI with the ones calculated by DCT are given in Table 5.2.

Considering Table 5.2, it can be observed that the results computed using the EDI method is in good agreement with the results of DCT. Finite element application of equivalent domain integral is explained in Chapter 4. All parameters in the integrand of (2.46) are calculated at every four Gauss Points of every element. Furthermore, during thermomechanical analysis, temperatures of all nodes are calculated first, and they are applied as external loads to structural elements. This coupled analysis requires a very fine mesh in order to produce accurate results. For this reason, the mesh inside and also outside of the integral domain around both crack tips are required to be very finely tuned.

Table 5.2 Normalized mixed-mode SIFs comparison, $\gamma_1 = 1.5, \gamma_2 = 1.5, \gamma_4 = 2.0$.

			EDI				*DCT*
			$R/a = 0.1$	$R/a = 0.2$	$R/a = 0.3$	$R/a = 0.4$	
$\phi = 0$	$\gamma_3 = 0.5$	$K_{In}(A)$	-0.0017	-0.0017	-0.0017	-0.0016	-0.0016
		$K_{IIn}(A)$	0.2108	0.2108	0.2108	0.2108	0.2096
		$K_{In}(B)$	0.0017	0.0021	0.0018	0.0016	0.0017
		$K_{IIn}(B)$	0.2108	0.2108	0.2108	0.2108	0.2096
	$\gamma_3 = 2$	$K_{In}(A)$	0.0011	0.0011	0.0011	0.0012	0.0012
		$K_{IIn}(A)$	0.1815	0.1815	0.1815	0.1815	0.1805
		$K_{In}(B)$	-0.0011	-0.0011	-0.0011	-0.0012	-0.0011
		$K_{IIn}(B)$	0.1815	0.1815	0.1815	0.1815	0.1805
$\phi = \frac{\pi}{6}$	$\gamma_3 = 0.5$	$K_{In}(A)$	0.0656	0.0672	0.0665	0.0670	0.0656
		$K_{IIn}(A)$	0.0977	0.0966	0.0971	0.0968	0.0972
		$K_{In}(B)$	-0.0812	-0.0819	-0.0816	-0.0836	-0.0814
		$K_{IIn}(B)$	0.3021	0.3019	0.3020	0.3014	0.3003
	$\gamma_3 = 2$	$K_{In}(A)$	0.0661	0.0677	0.0677	0.0675	0.0671
		$K_{IIn}(A)$	0.0692	0.0677	0.0677	0.0675	0.0680
		$K_{In}(B)$	-0.0801	-0.0805	-0.0802	-0.0801	-0.0804
		$K_{IIn}(B)$	0.2685	0.2684	0.2679	0.2675	0.2668
$\phi = \frac{\pi}{3}$	$\gamma_3 = 0.5$	$K_{In}(A)$	0.1178	0.1173	0.1170	0.1172	0.1178
		$K_{IIn}(A)$	0.0571	0.0583	0.0590	0.0585	0.0570
		$K_{In}(B)$	-0.2377	-0.2384	-0.2458	-0.2409	-0.2373
		$K_{IIn}(B)$	0.2105	0.2100	0.2100	0.2067	0.2100
	$\gamma_3 = 2$	$K_{In}(A)$	0.1291	0.1289	0.1290	0.1290	0.1290
		$K_{IIn}(A)$	0.0346	0.0352	0.0355	0.0352	0.0346
		$K_{In}(B)$	-0.2197	-0.2170	-0.2252	-0.2121	-0.2194
		$K_{IIn}(B)$	0.1849	0.1888	0.1781	0.1935	0.1840
$\phi = \frac{\pi}{2}$	$\gamma_3 = 0.5$	$K_{In}(A)$	0.1143	0.1141	0.1140	0.1141	0.1142
		$K_{IIn}(A)$	0.0000	0.0000	0.0000	0.0000	0.0000
		$K_{In}(B)$	-0.2997	-0.2996	-0.2996	-0.2996	-0.2996
		$K_{IIn}(B)$	0.0000	0.0000	0.0000	0.00000	0.00000
	$\gamma_3 = 2$	$K_{In}(A)$	0.1325	0.1325	0.1325	0.1325	0.1325
		$K_{IIn}(A)$	0.0000	0.0000	0.0000	0.0000	0.0000
		$K_{In}(B)$	-0.2727	-0.2727	-0.2727	-0.2727	-0.2726
		$K_{IIn}(B)$	0.0000	0.0000	0.0000	0.0000	0.0000

When the results of each domain size is examined, EDI results for corresponding domain sizes are very close to eachother. Therefore, it can be concluded that the results of EDI analysis are domain independent. This property of J_k - integral is explained in Chapter 2. All of the calculated SIF values are within 1% error range with respect to their corresponding DCT and domain size values.

The need for very fine meshes drives the runtimes of equivalent domain integral to be considerably much longer than that of displacement correlation technique. In Table 5.2, four different domain sizes, being $R/a = 0.1$, 0.2, 0.3 and 0.4 are used to compute the stress intensity factor by means of the EDI technique. For small region calculations, $R/a = 0.1$, number of elements required to reach an accurate result is nearly 17,000. The runtimes for $R/a = 0.1$ is nearly 3 hours, whereas DCT runtime for the same mesh is 15 minutes. As the domain of integral is enlarged, the number of elements required to access an accurate result increases. Therefore, as the region is enlarged, the mesh inside and also outside of the domain is increased. For example, as the domain is enlarged to $R/a = 0.4$, the number of elements to calculate the SIF's increases to 40,000 The discussions about runtimes and domain sizes is summarized in Table 5.3.

Table 5.3 Total number of elements utilized for different domain size and corresponding runtimes

Domain Size	*Total Number of Elements*	*Runtime*
$R/a = 0.1$	17,000	3 hours
$R/a = 0.2$	20,000	6 hours
$R/a = 0.3$	24,000	12 hours
$R/a = 0.4$	40,000	18 hours

5.2.3 Variations in the Thermal Expansion Coefficient

In this section, the results regarding various nonhomogeneity constant of thermal expansion coefficient γ_3 are presented. Thermal expansion coefficient of FGM layer changes throughout the layer according to the function given by (3.1.c). In order to investigate the response of the FGM layer to varying γ_3 values, several graphics are plotted. When γ_3 takes the value of 1.0, the thermal expansion coefficient varies linearly through the FGM layer. When γ_3 reaches to infinity**,** thermal expansion coefficient of ceramic material is dominant. Variations in the Mode I and Mode II thermal SIF's of crack tip, A, for different nonhomogeneity constants of thermal expansion coefficient γ_3 are shown in Figure 5.15 and Figure 5.16, respectively.

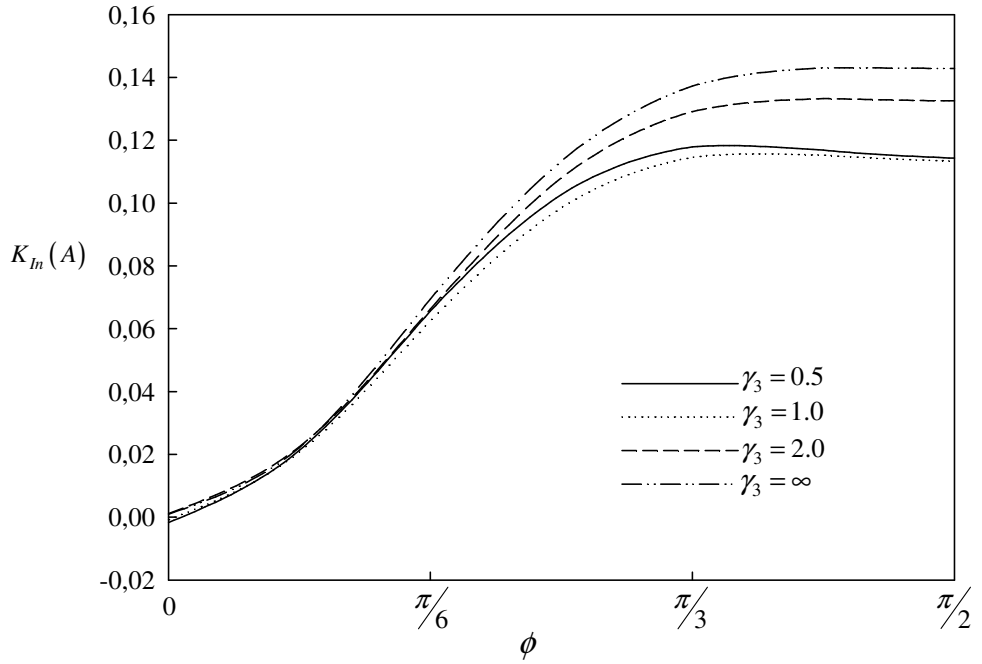

Figure 5.15 Normalized Mode I Stress Intensity Factors of crack tip A versus angle of crack, $a/W = 0.1$, $h_2/a = 2.0$, $h_1/a = 2.0$, $\gamma_1 = \gamma_2 = 1.5$, $\gamma_4 = 2.0$

Mode I SIF approaches zero for every γ_3 value at an angle of $\phi = 0$, and increases as ϕ is increased from 0 to $\phi = \pi/2$.

On the contrary, Mode II SIF exactly equals zero at the angle of $\phi = \pi/2$ regardless of the thermal expansion coefficient behavior. This is due to the fact that, the problem turns into a Mode I problem when the angle of crack equals $\pi/2$. Mode II SIF's take a maximum value at the angle of $\phi = 0$.

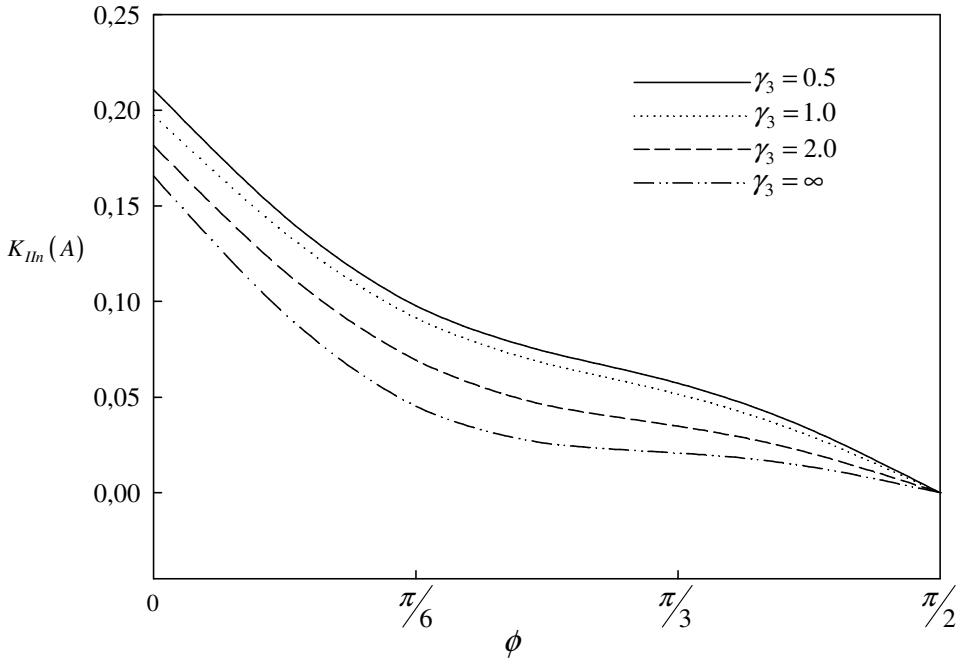

Figure 5.16 Normalized Mode II Stress Intensity Factors of crack tip A versus angle of crack, $a/W = 0.1$, $h_2/a = 2.0$, $h_1/a = 2.0$, $\gamma_1 = \gamma_2 = 1.5$, $\gamma_4 = 2.0$

The behavior of Mode I and Mode II thermal SIF's of crack tip B for different nonhomogeneity constants of thermal expansion coefficient γ_3 are shown in Figure 5.17 and Figure 5.18.

Mode I SIF for crack tip *B* are approximately zero for all thermal expansion coefficient values at angle of $\phi = 0$. It can be observed from Figure 5.17 that all Mode I SIF's possess negative values. This means that crack closure occurs near crack tip *B*, while crack tip *A* experiences a crack opening phenomena.

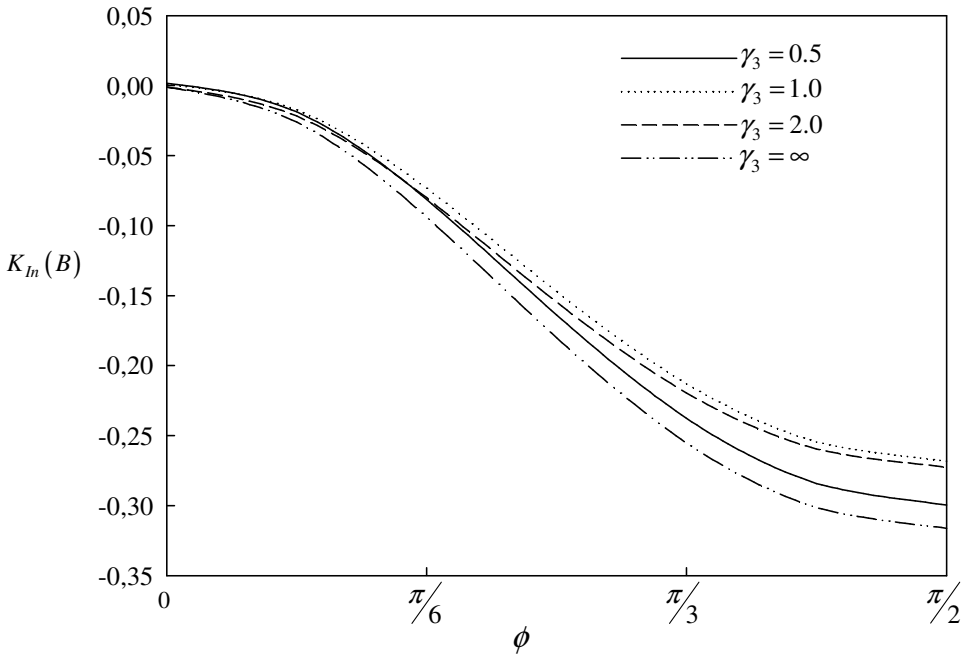

Figure 5.17 Normalized Mode I Stress Intensity Factors of crack tip B versus angle of crack, $a/W = 0.1$, $h_2/a = 2.0$, $h_1/a = 2.0$, $\gamma_1 = \gamma_2 = 1.5$, $\gamma_4 = 2.0$

Mode II SIF's end up with exactly zero value at the angle of $\phi = \pi/2$, while making a peak around $\pi/6$. For metal rich thermal expansion coefficient behavior Mode II SIF takes its maximum value.

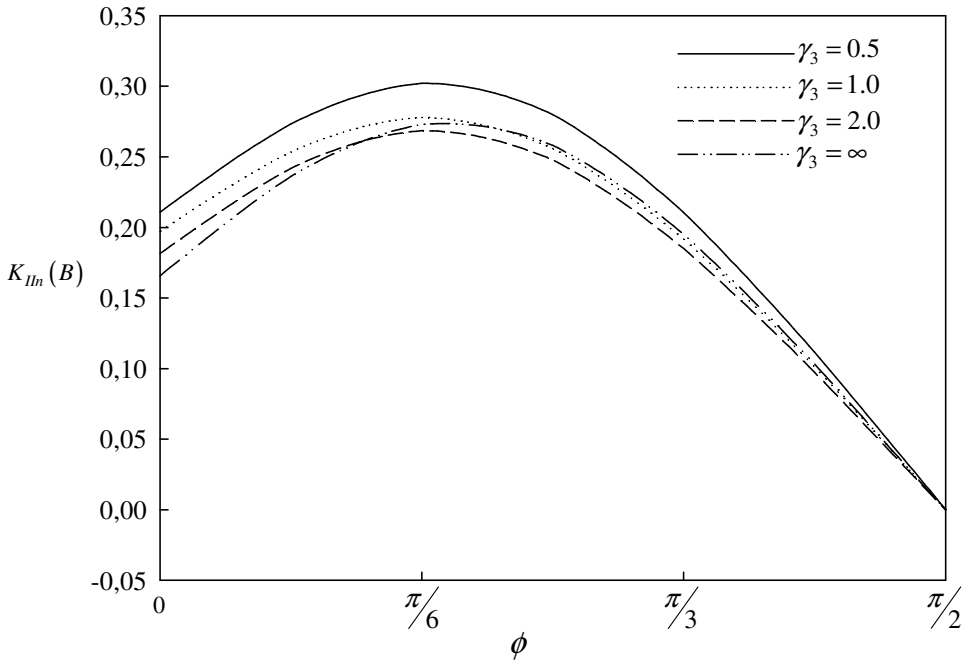

Figure 5.18 Normalized Mode II Stress Intensity Factors of crack tip B versus angle of crack, $a/W = 0.1$, $h_2/a = 2.0$, $h_1/a = 2.0$, $\gamma_1 = \gamma_2 = 1.5$, $\gamma_4 = 2.0$

One of the most appreciable aspects of the evaluation of SIF's by equivalent domain integral method is that T-stress calculation is possible. By utilizing the simple equation introduced in (2.83), T-stresses at both crack tips can be calculated.

In Figure 5.19, it can be observed that, T-stress values are positive for upper crack tip A nearly upto a crack angle of $\phi = \pi/6$, for all values of γ_3. For crack angles larger than $\phi = \pi/6$, T-stress values become negative and make a minimum at about $\phi = \pi/3$. For angle of cracks larger than $\phi = \pi/3$, T-stress values tend to increase for $\gamma_3 = 0.5$ and $\gamma_3 = 1.0$.

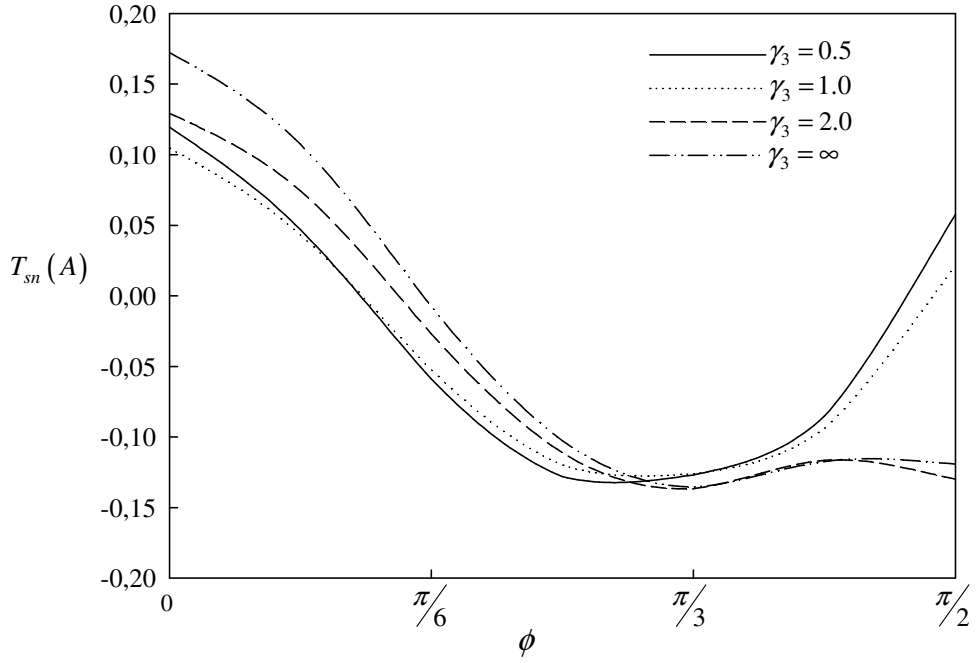

Figure 5.19 Normalized T - stress of crack tip A versus angle of crack $a/W = 0.1$, $h_2/a = 2.0$, $h_1/a = 2.0$, $\gamma_1 = \gamma_2 = 1.5$, $\gamma_4 = 2.0$

T-stress values are plotted for crack tip B in Figure 5.20. T-stress becomes minimum for crack angle of $\phi = 0$. At an angle of $\phi = \pi/4$, all of the T-stress values equal to zero, regardless of γ_3 value. This means that the asymptotic stress expression given in APPENDIX B does not have any T-stress contribution. Stress field is driven by only Mode I and Mode II SIF's. T-stress values tend to increase upto an angle of approximately $\phi = 5\pi/12$, at which point there is a minimum. For metallic thermal expansion coefficient behavior, T-stress value for angle of $\phi = 0$ is minimum and for angle of $\phi = \pi/2$ is maximum.

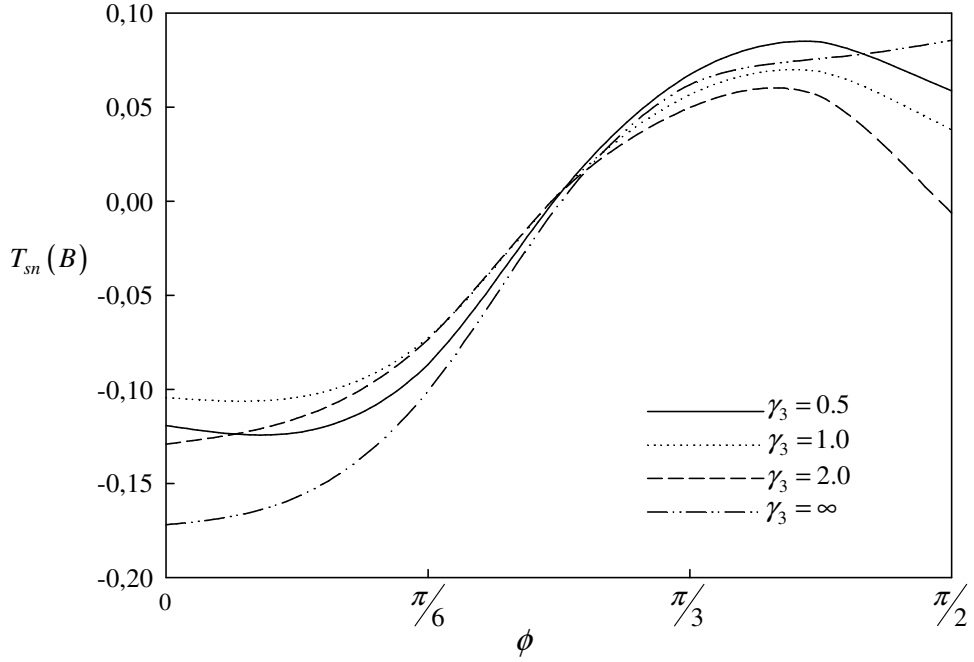

Figure 5.20 Normalized T - stress of crack tip B versus angle of crack $a/W = 0.1,\ h_2/a = 2.0,\ h_1/a = 2.0, \gamma_1 = \gamma_2 = 1.5,\ \gamma_4 = 2.0$

5.2.4 Variations in the Thermal Conductivity

Heat conduction refers to the transport of energy in a medium due to a temperature gradient. Thermal conductivity is referred as a transport property, which provides an indication of the rate at which energy is transferred by the diffusion process. Thermal conductivity simply depends on the state of the matter.

In this study, upper and lower boundaries are kept at temperatures of $T_1 = 2*T_0$ and $T_2 = T_0$, respectively. For this prescribed boundary conditions, the conduction heat flux increases with increasing thermal conductivity. This section is dedicated to the results regarding the varying nonhomogeneity constant of thermal conductivity γ_4. The thermal conductivity of the FGM layer change throughout the layer by the function given by (3.1.d).

Steady state temperature distribution for various values of the nonhomogeneity parameter of thermal conductivity, γ_4 are computed. For both crack tips *A* and *B* the temperature distributions are presented in Figure 5.21 and 5.22, respectively.

As the angle of crack is increased while keeping the crack length constant, the crack tip *A* comes closer to the upper surface which has $T = 2*T_0$. This means that, as the crack tip comes closer to the surface, the temperature of the crack tip *A* increases. As expected, when the angle of crack is $\pi/2$, the temperature reaches its maximum for all of the γ_4 values.

In contrast to the behavior of crack tip *A*, crack tip *B* experiences a temperature drop as the angle of crack increases. This is simply due to the fact that, crack tip *B* gets closer to the lower surface of the layer, which has a steady-state temperature of $T = T_0$.

As the crack tip *B* gets closer, it gets into cooler regions. It can be observed from Figure 5.22 that temperature at crack tip *B* decreases as the angle of crack is increased and for an angle of crack, $\phi = \pi/2$ it reaches its minimum value. When $\gamma_4 \to \infty$, the material distribution becomes ceramic rich. For this case, thermal conductivity of ceramic material is dominant. In this material distribution case, temperature values of crack tip *A* and crack tip *B* for all angles are higher than any other γ_4 case.

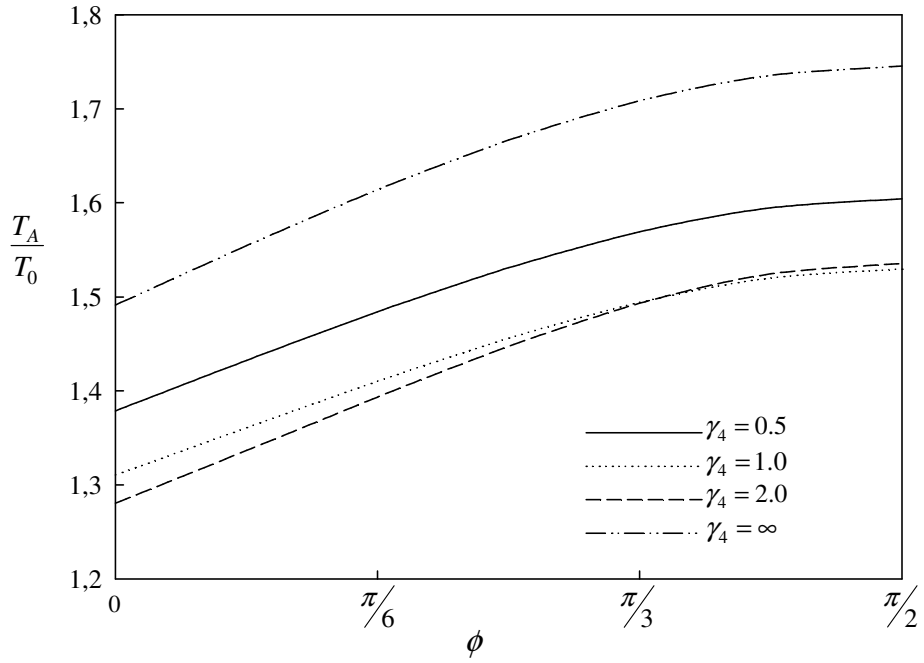

Figure 5.21 Temperature distribution of the crack tip A
$a/W = 0.1$, $h_2/a = 2.0$, $h_1/a = 2.0$ $\gamma_1 = \gamma_2 = 1.5$, $\gamma_3 = 2.0$

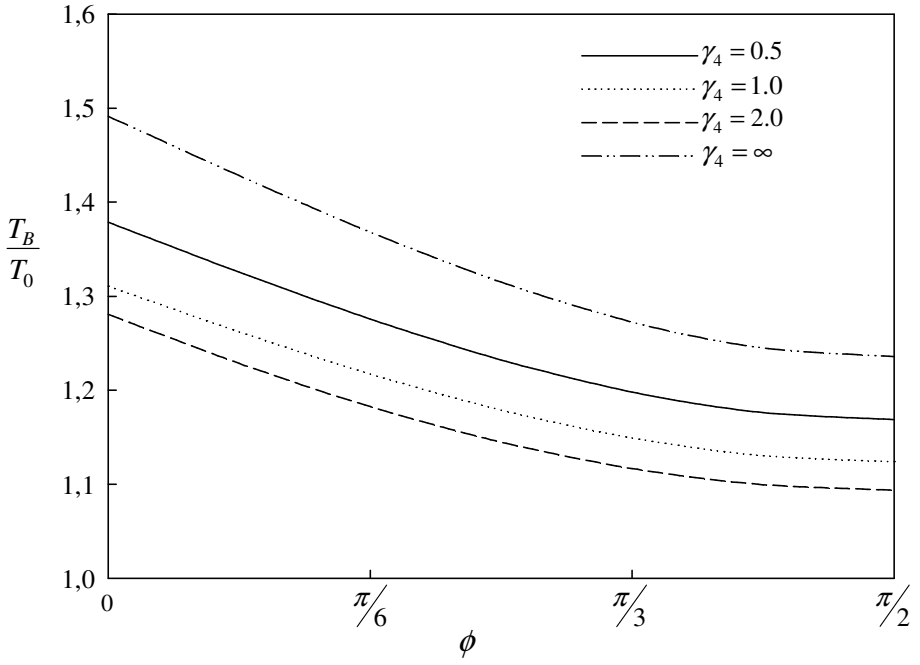

Figure 5.22 Temperature distribution of the crack tip B, $a/W = 0.1,\ h_2/a = 2.0,\ h_1/a = 2.0, \gamma_1 = \gamma_2 = 1.5,\ \gamma_3 = 2.0$

The behavior of Mode I and Mode II thermal SIF's at crack tip A, for different nonhomogeneity constants of thermal conductivity γ_4 are plotted in Figure 5.23 and Figure 5.24, respectively.

Regarding the range of thermal conductivity behavior $0.5 \le \gamma_4 \le 2.0$, Mode I SIF of crack tip *A* takes its minimum value at an angle of $\phi = 0$. The Mode I SIF tends to increase as the angle of crack is increased. Mode I SIF takes its maximum values at $\phi = \pi/2$. Moreover, Mode I SIF always takes positive values for material property distributions of the range $0.5 \le \gamma_4 \le 2.0$. This simply means that, crack tip *A* opens as the angle of crack is increased under the previously specified thermal conditions.

When the material behavior of thermal conductivity becomes ceramic dominant, every tendency of the Mode I SIF turns vice versa. Therefore, Mode I SIF takes a minimum value at $\phi = \pi/2$ and at this point crack closure can be observed.

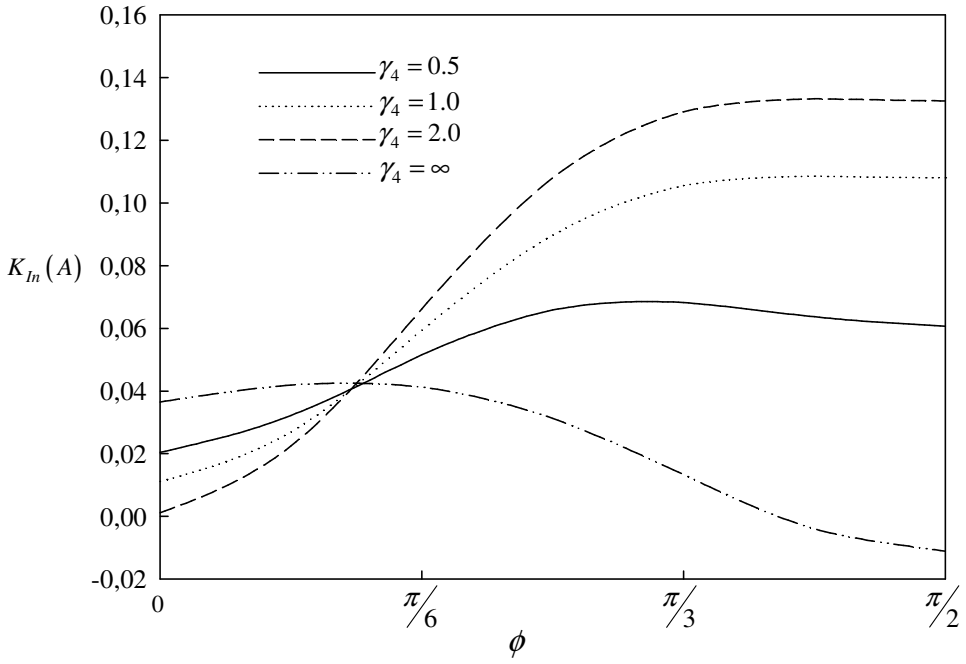

Figure 5.23 Normalized Mode I Stress Intensity Factors of crack tip A versus angle of crack, $a/W = 0.1$, $h_2/a = 2.0$, $h_1/a = 2.0$, $\gamma_1 = \gamma_2 = 1.5$, $\gamma_3 = 2.0$

When the Mode II SIF of crack tip *A* is analyzed, it is observed in Figure 5.24 that it exactly equals to zero at $\phi = \pi/2$, regardless of the γ_4 value. This is an expected result and a checkpoint for the conducted analysis. When $\phi = \pi/2$, the problem is a simply Mode I problem and the Mode II SIF's are exactly zero.

For every γ_4 value, Mode II SIF takes its maximum value at $\phi = 0$ and tends to decrease as the angle of crack is increased. This is also an expected aspect of the problem, Mode II SIF contribution to the problem is more dominant in this case of orientation angle.

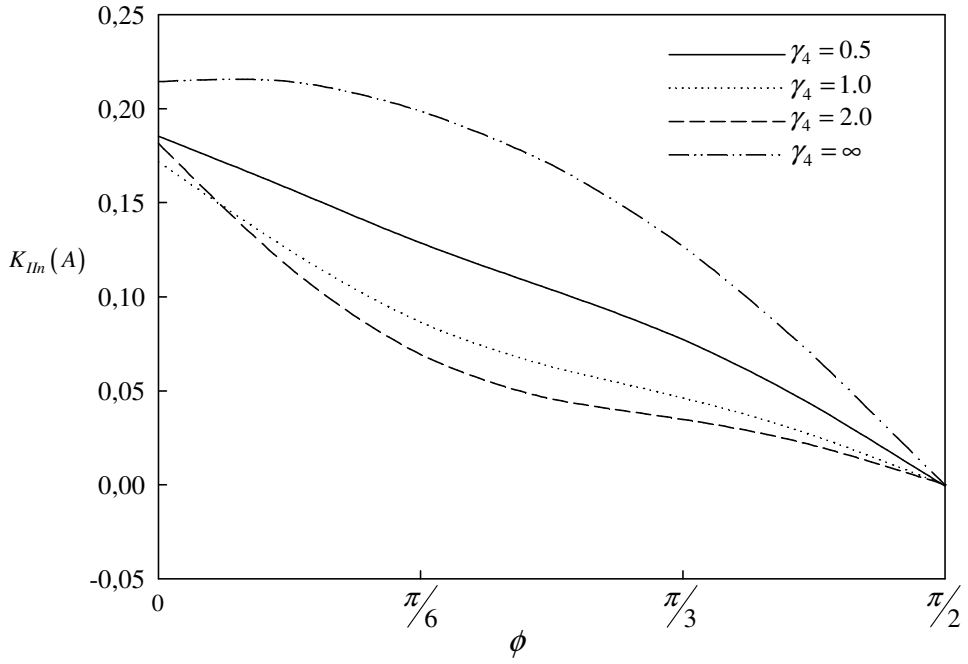

Figure 5.24 Normalized Mode II Stress Intensity Factors of crack tip A versus angle of crack, $a/W = 0.1$, $h_2/a = 2.0$, $h_1/a = 2.0$, $\gamma_1 = \gamma_2 = 1.5$, $\gamma_3 = 2.0$

Figure 5.25 presents that the Mode I SIF of crack tip *B*, takes its maximum value at $\phi = 0$ for cases of $0.5 \le \gamma_4 \le 2.0$. This maximum value is negative, which implies that crack closure always takes place regardless of the value of the crack angle. At the angle of $\phi = \pi/2$, it takes its minimum value for $0.5 \le \gamma_4 \le 2.0$.

For the case of $\gamma_4 \to \infty$, the scenario completely changes. When the angle of crack is $\phi = \pi/6$, Mode I SIF of crack tip *B* becomes zero for larger values of ϕ, it becomes positive, meaning that crack is opened.

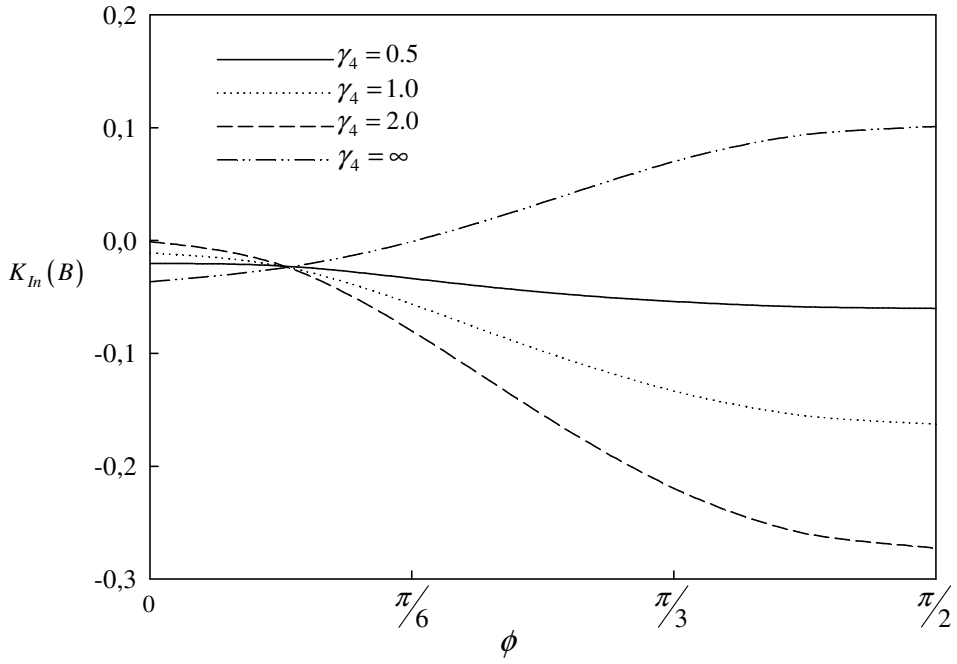

Figure 5.25 Normalized Mode I Stress Intensity Factors of crack tip B versus angle of crack, $a/W = 0.1$, $h_2/a = 2.0$, $h_1/a = 2.0$, $\gamma_1 = \gamma_2 = 1.5$, $\gamma_3 = 2.0$

Mode II SIF for crack tip *B* equals exactly zero for the case of $\phi = \pi/2$ just like crack tip *A* as illustrated in Figure 5.26. Purely Mode I behavior is observed in this case.

When Figure 5.26 and Figure 5.18 are compared, it is noted that Mode II SIF increases steeper than that of thermal conductivity and both of the plots tend to have a maximum at about angles $\phi = \pi/6$. When $\gamma_4 \approx 0$, metallic thermal conductivity behavior is dominant. As metallic behavior gets more dominant, Mode II SIF's tend to decrease.

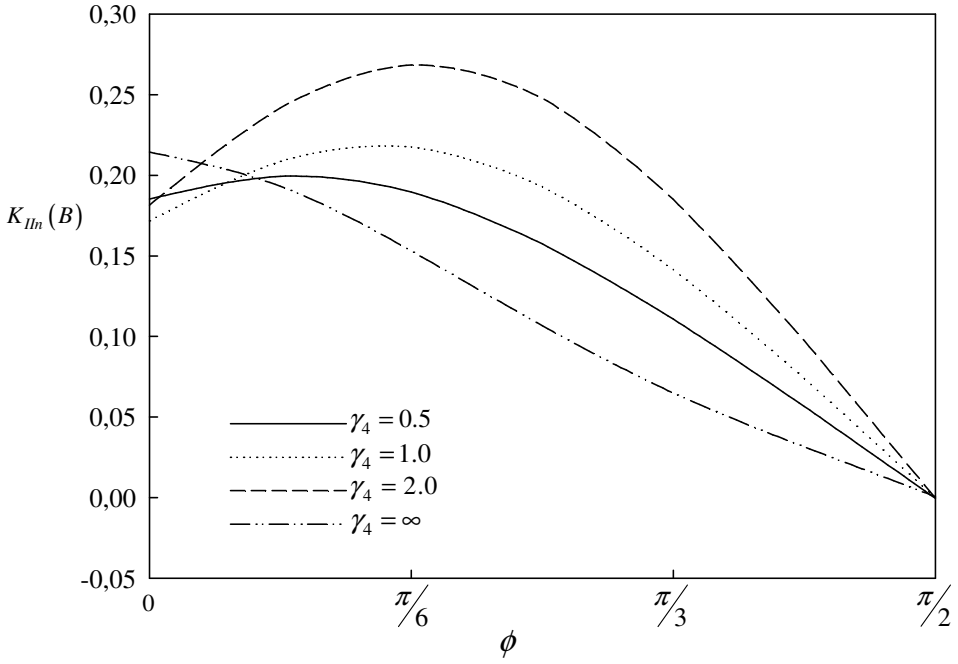

Figure 5.26 Normalized Mode II Stress Intensity Factors of crack tip B versus angle of crack, $a/W = 0.1$, $h_2/a = 2.0$, $h_1/a = 2.0$, $\gamma_1 = \gamma_2 = 1.5$, $\gamma_3 = 2.0$

T -stress values for crack tip A are presented in Figure 5.27. It can be concluded from the figure that, as metallic behavior gets more dominant, T -stress values change in a more narrow range. T -stress values make a maximum at $\phi = 0$. When the tendency of ceramic rich behavior is analyzed, T -stress values for angle of $\phi = 0$ tend to increase more and more.

In the analyses for thermal expansion coefficient which is plotted previously in Figure 5.19, T -stress values for all γ_3 values are close to each other. Coarsely, this behavior can be commented as T -stress is insensitive to γ_3 values for angle range of $0 \le \phi \le \pi/3$.

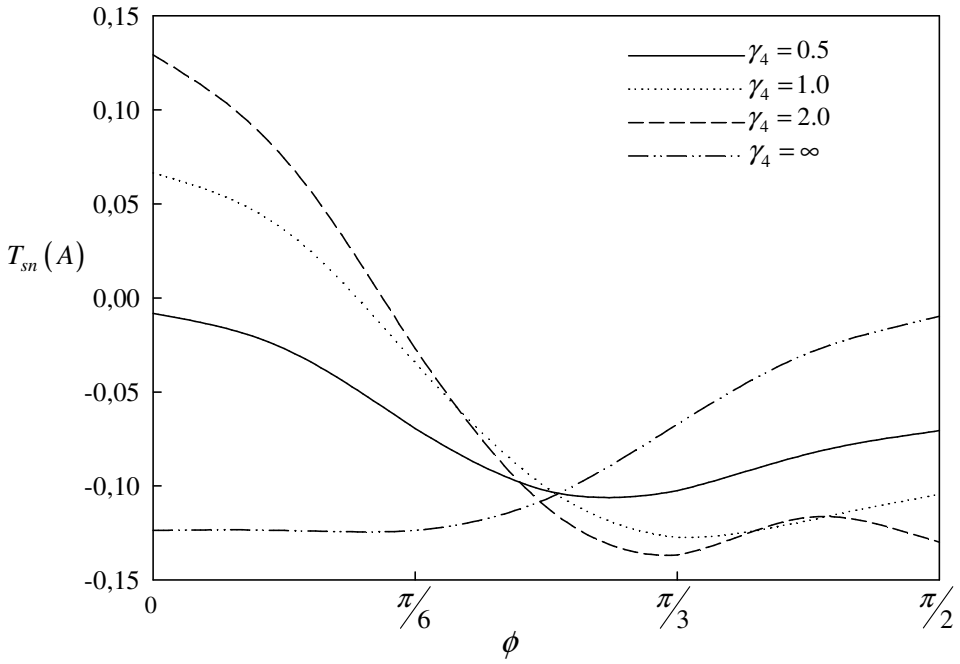

Figure 5.27 Normalized T - stress of crack tip A versus angle of crack, $a/W = 0.1$, $h_2/a = 2.0$, $h_1/a = 2.0$, $\gamma_1 = \gamma_2 = 1.5$, $\gamma_3 = 2.0$

T -stress values of crack tip B for different thermal conductivity cases is plotted in Figure 5.28. As the metallic thermal conductivity behavior gets more dominant in the analyses, T -stress values deviate around zero. It can be concluded that purely metallic behavior of thermal conductivity results in approximately zero T -stress. Therefore, T -stress component of asymptotic stresses can be neglected for this cases. Moreover, embedded crack problems having $\phi = \pi/4$ have T -stress values that are exactly equal to zero, irrespective of the thermal conductivity behavior. Asymptotic stresses can be expressed in terms of Mode I and Mode II SIF's only in this case. This trend is also observed for different γ_4 values which are illustrated in Figure 5.20.

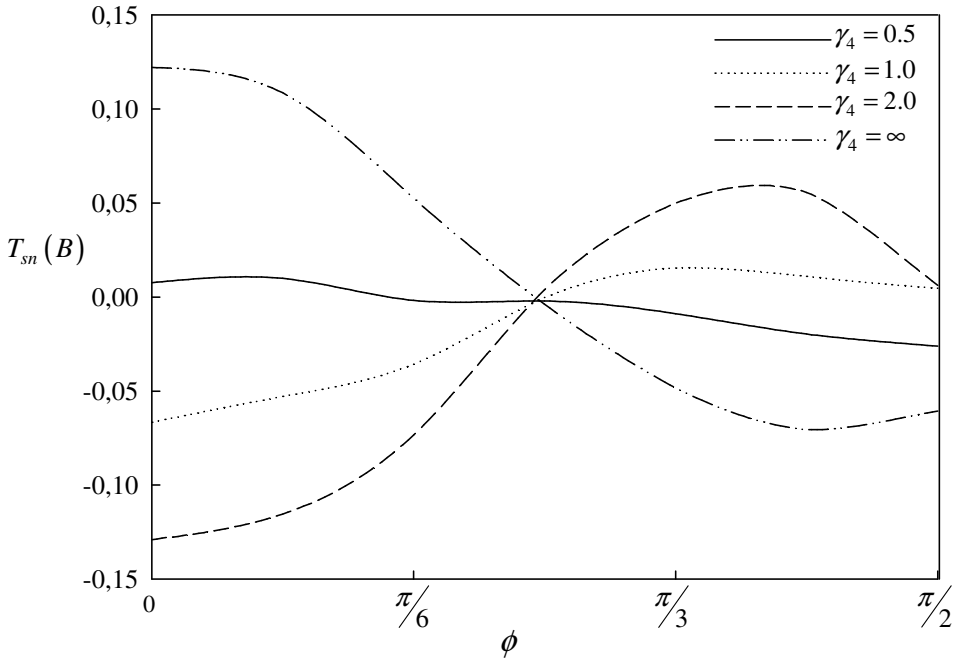

Figure 5.28 Normalized T - stress of crack tip B versus angle of crack, $a/W = 0.1$, $h_2/a = 2.0$, $h_1/a = 2.0$, $\gamma_1 = \gamma_2 = 1.5$, $\gamma_3 = 2.0$

CHAPTER 6

CONCLUDING REMARKS

In this study, a computational method based on the generalized definition of *J*-integral is developed to study crack problems in isotropic FGM's under thermal stresses. Path independent J-integral is converted to an Equivalent Domain Integral that can be calculated over an arbitrary area around the crack tip. The developed formulation is integrated in a commercial finite element analysis tool. Thermal and structural problems are modelled and solved by applying two-step analysis.

The problem of horizontal edge crack under thermomechanical loading is analyzed in order to verify the accuracy of EDI technique. The developed procedure is validated by comparing results of stress intensity factors to those reported in the literature. The results obtained using the equivalent domain integral approach is shown to be highly accurate and independent of domain size used in the finite element computations.

The problem of inclined embedded crack in isotropic Functionally Graded Medium have been analyzed in this study. The Functionally Graded Medium is a bulk layer, that is material distribution changes throughout the layer. This study verifies the domain independence of J_k-integral and accuracy of Equivalent Domain Integral is proven.

Mode I and Mode II stress intensity factors at both crack tips of the embedded crack are calculated. Additionally, T-stress values for both of the crack tips are extracted. T-stress can not be calculated with the use of displacement correlation technique. However, T-stress values can be calculated with the use of EDI

technique. Effects of variations in thermal expansion coefficient and thermal conductivity on these fracture parameters are presented graphically.

The results are quite accurate; however, they may be improved by utilizing some other properties of finite element approach. In this study, material properties are assigned to the centroids of each element. During finite element preprocessing stage, the material properties can be assigned to more than one point inside one element. This approach could extensively improve the accuracy of the results. As the number of material property application points are increased, Functionally Graded Material behavior can be analyzed more accurately. The results can also be finely tuned when the mesh inside and outside the crack tip domains are refined. As the mesh is defined with more elements, the obtained results become pretty accurate. However, this requires a very good configuration of computing devices and software. One of the limiting aspects of utilizing very fine meshes is that runtimes for very fine meshes could also reach up to one day.

The problems solved in this study are theoretical models, therefore they are not applied problems in reality. This work can be extended for realistic problems such as inclined edge cracks in FGM coatings that are bonded to a homogenous substrate. Future work could be focused on the analysis of steady-state and transient thermal loading on FGM coating and substrate systems. Boundary conditions could also be changed such that crack faces could experience partial insulation. Moreover, variations in other thermomechanical material properties could be analyzed, such as Poisson's ratio. In this study, Poisson's ratio is assumed to be constant throughout the FGM layer. The effect of variations in this material property parameter is investigated in the literature and reported to have significant effect on fracture behavior for certain cases. Additionally, this work is formulated for plane strain case. The formulation could be oriented such that it is possible to solve for plane stress problems.

REFERENCES

[1] Kim J.H., Paulino G.H., 2003. "Mixed-mode *J*-integral formulation and implementation using graded elements for fracture analysis of nonhomogeneous orthotropic materials", *Mech Mater*, Vol 35, pp.107-128

[2] Kim J.H., Paulino G.H., 2002. "Isoparametric graded finite elements for nonhomogenous isotropic and orthotropic materials", *ASME J Appl Mech*, Vol. 69, pp.502-514

[3] Rice J.R.,1968. "A path independent integral and approximate analysis of strain concentration by notches and cracks", *J Appl Mech*, Vol 35, pp. 379-386

[4] Gu P., Dao M., Asaro R.J.,1999. "A simplified Method for calculating the crack-tip field of functionally graded materials using the domain integral", *J Appl Mech*, Vol 66, pp. 101-108

[5] Dağ S., Yıldırım B., Erdoğan F., 2004. "Interface crack problems in graded orthotropic media: analytical and computational approaches", *Int J Fract*, Vol 130, pp. 471-49

[6] Kim J.H., Paulino G.H., 2002. "Finite element evaluation of mixed mode stress intensity factors in functionally graded materials", *Int J Numer Methods Eng,* Vol 53, pp.1903-1935

[7] Kim J.H., Paulino G.H., 2001. "Mixed mode fracture of orthotropic functionally graded materials using finite elements and the modified crack closure method". *Engng Fract Mech,* Vol 69, pp.1557-1586

[8] Yıldırım B., Dağ S., Erdoğan F., 2005. "Three dimensional fracture analysis of FGM coatings under thermomechanical loading", *Int J Fract*, Vol 132, pp. 369-395

[9] Paulino G.H., Kim J.H., 2004. "A new approach to compute T –stress in functionally graded materials by means of the interaction integral method", *Engng Fract Mech*, Vol 71, pp.1907-1950

[10] Larsson S.G, Carlson A.J., 1973 "Influence of non-singular stress terms and specimen geometry on small-scale yielding at crack-tips in elastic–plastic materials", *J Mechs Phys Solids* , Vol 21, pp.263-277

[11] ANSYS User's Guide

[12] Eshelby J.D., 1970. "The energy momentum tensor in continuum mechanics", *Inelastic Behavior of Solids* (Edited by M.F. Kanninen et al.) pp. 77-114. McGraw-Hill, New York

[13] Dağ S., 2006. "Thermal Fracture analysis of orthotropic functionally graded materials using an equivalent domain integral approach" *Engng Fract Mech*, Vol 73, pp.2802–2828

[14] Dağ S., 2006. "Mixed-mode fracture analysis of functionally graded materials under thermal stresses: A new approach using J_k -integral" accepted for publication in *J Therm Stresses*

[15] Reddy J.N., *"An introduction to the Finite Element Method"* 3rd Edition, McGraw Hill, 2006

[16] Walters M.C, Paulino G.H., Dodds R.H. Jr., 2004. "Stress-intensity factors for surface cracks in functionally graded materials under mode-I thermomechanical loading". *Int J Solids Struct*, Vol 41, pp.1081–1118

[17] Erdogan F., Wu B.H., 1996. "Crack problems in FGM layers under thermal stresses". *J Therm Stresses*, Vol 19, pp. 237-265

[18] Yılmaz S., "Buckling driven delamination of orthotropic functionally graded materials." MS- Thesis, METU, 2006

APPENDIX A

DIVERGENCE THEOREM

Let ∇ denote the Del Operator in the two-dimensional Cartesian rectangular coordinate system *(x, y)* as shown in Figure A.1,

$$\nabla = \hat{e}_x \frac{\partial}{\partial x} + \hat{e}_y \frac{\partial}{\partial y} \tag{A.1}$$

where $\hat{e}_x$ and $\hat{e}_y$ denote the unit vectors along x and y coordinates, respectively.

If $\vec{G}(x, y)$ is a vector function of class $C^0(\Omega)$ in the domain Ω shown in the Figure A.1, the following divergence theorem holds.

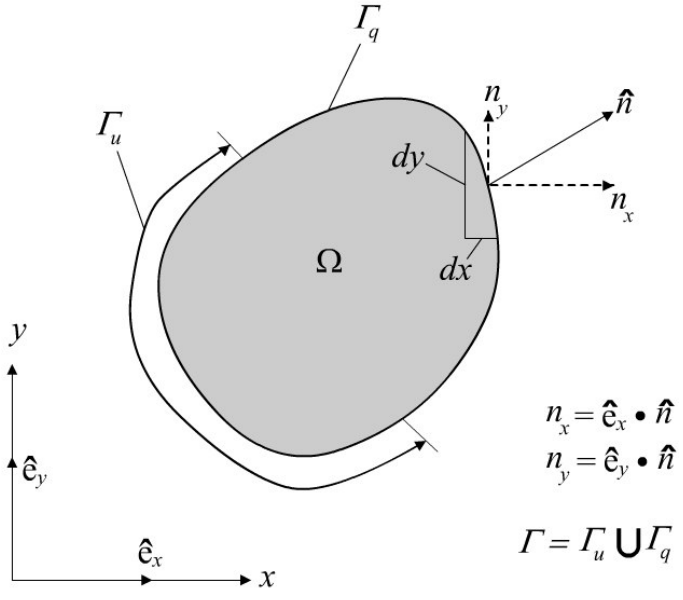

Figure A.1 Divergence theorem in two dimensional domain

$$\int_{\Omega} div\vec{G}\, dx\, dy \equiv \int_{\Omega} \vec{\nabla} \cdot \vec{G}\, dx\, dy = \oint_{\Gamma} \hat{n} \cdot \vec{G}\, ds \tag{A.2}$$

where, unit normal can be represented as $\vec{n} = n_x \hat{i} + n_y \hat{j}$

vector function can be represented as $\vec{G} = G_x \hat{i} + G_y \hat{j}$

$$\int_{\Omega} \left(\frac{\partial G_x}{\partial x} + \frac{\partial G_y}{\partial y} \right) dx\, dy = \oint_{\Gamma} \left(n_x\, G_x + n_y\, G_y \right) ds \tag{A.3}$$

or in indicial notation,

$$\int_{\Omega} \left(\frac{\partial G_i}{\partial x_i} \right) dx_i\, dx_j = \oint_{\Gamma} \left(n_i\, G_i \right) ds \tag{A.4}$$

Here the dot denotes the scalar product of vectors, $\hat{n}$ denotes the unit vector normal to the surface Γ of the domain Ω; n_x and n_y (G_x and G_y) are the rectangular components of $\hat{n}(G)$; and the circle on the boundary integral indicates that the integration is taken over the entire boundary.

APPENDIX B

ASYMPTOTIC EXPRESSIONS FOR STRESS COMPONENTS

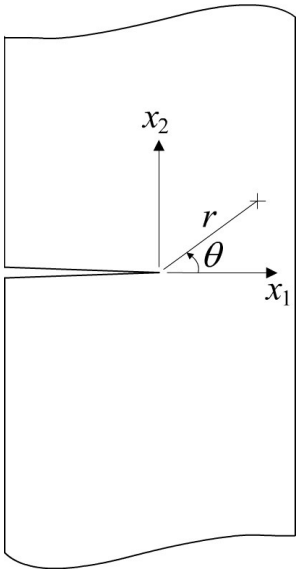

Figure B.1 Crack tip coordinate system transformation

For a crack seen in the Figure B.1, one can write the asymptotic stress expressions as follows,

$$\sigma_{ij}(r,\theta) = \frac{K_I}{\sqrt{2\pi r}} f_{ij}^{I}(\theta) + \frac{K_{II}}{\sqrt{2\pi r}} f_{ij}^{II}(\theta) + T_s \delta_{1i} \delta_{1j} \qquad \textbf{(B.1)}$$

where T_s is the non-singular stress, or so called *T*-stress.

The explicit form of asymptotic representations is as follows,

$$\sigma_{11}(r,\theta)=\frac{K_I}{\sqrt{2\pi r}}\cos\frac{\theta}{2}\left\{1-\sin\frac{\theta}{2}\sin\frac{3\theta}{2}\right\}-\frac{K_{II}}{\sqrt{2\pi r}}\sin\frac{\theta}{2}\left\{2+\cos\frac{\theta}{2}\cos\frac{3\theta}{2}\right\}+T_s$$

$$\sigma_{22}(r,\theta)=\frac{K_I}{\sqrt{2\pi r}}\cos\frac{\theta}{2}\left\{1+\sin\frac{\theta}{2}\sin\frac{3\theta}{2}\right\}+\frac{K_{II}}{\sqrt{2\pi r}}\sin\frac{\theta}{2}\cos\frac{\theta}{2}\cos\frac{3\theta}{2} \qquad \textbf{(B.2)}$$

$$\sigma_{12}(r,\theta)=\frac{K_I}{\sqrt{2\pi r}}\sin\frac{\theta}{2}\cos\frac{\theta}{2}\cos\frac{3\theta}{2}+\frac{K_{II}}{\sqrt{2\pi r}}\cos\frac{\theta}{2}\left\{1-\sin\frac{\theta}{2}\sin\frac{3\theta}{2}\right\}$$

APPENDIX C

q FUNCTION

C.1 Circular region around the crack tip

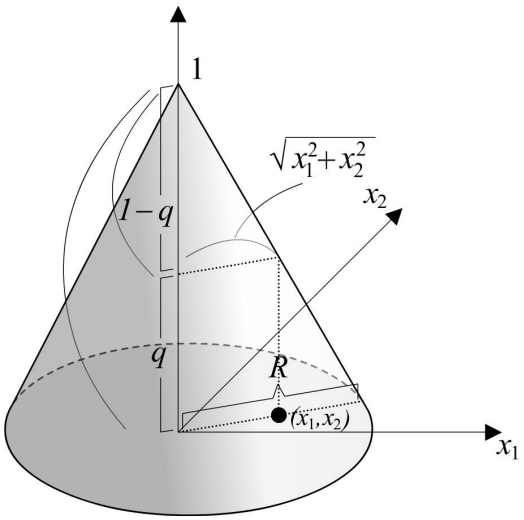

Figure C.1 Orientation of the *q*- function

$$\frac{\sqrt{x_1^2+x_2^2}}{R}=\frac{1-q}{1} \Rightarrow \qquad q=1-\frac{\sqrt{x_1^2+x_2^2}}{R} \tag{C.1}$$

The derivatives of the q- function with respect to coordinates,

$$q_{,1}=-\frac{x_1}{R\sqrt{x_1^2+x_2^2}} \tag{C.2}$$

$$q_{,2}=-\frac{x_2}{R\sqrt{x_1^2+x_2^2}} \tag{C.3}$$

It is clear in the Figure C.2 that,

$$\frac{q}{1} = \frac{x}{R} \qquad \Rightarrow \qquad q = \frac{x}{R} \tag{C.4}$$

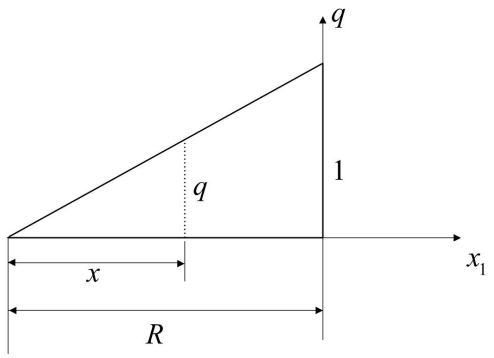

Figure C.2 *q*- function for a circular path around the crack tip

C.2 Rectangular region around the crack tip

$$q = 1 + \frac{x_1}{R} \qquad x - x_1 = R \tag{C.5}$$

Combining the two relations,

$$q = 1 + \frac{x - R}{R} \qquad \Rightarrow \qquad q = \frac{x}{R} \tag{C.6}$$

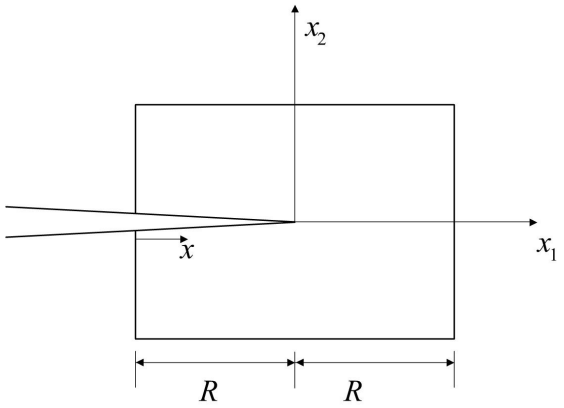

Figure C.3 *q*- function for a rectangular path around the crack tip